Dynamic susceptibility contrast MRI calibrated using T1-based steady-state CBV and vascular space occupancy (VASO): Comparison with model-free arterial spin labelling

Emelie Lindgren

Supervisors: Linda Knutsson and Ronnie Wirestam
Master of Science Thesis in Medical Radiation Physics, 30 credits
Department of Medical Radiation Physics, Lund University, Lund, Sweden

Abstract

Introduction

The perfusion-related parameters cerebral blood flow (CBF) and cerebral blood volume (CBV) can be measured using dynamic susceptibility-contrast magnetic resonance imaging (DSC-MRI). However, absolute values of CBF and CBV are often overestimated and quantification of these parameters is challenging. By acquiring an independent absolute CBV estimate, a calibration factor can be obtained by comparing these values with CBV values estimated with DSC-MRI. This calibration factor is theoretically applicable both to CBV and CBF obtained from the same DSC-MRI measurement. In this study, DSC-MRI-based CBV and CBF were calibrated using steady-state T1-based CBV (called Bookend) and vascular space occupancy (VASO) techniques, and calibrated CBF values were compared with CBF values obtained by arterial spin labelling (ASL) MRI.

Material and Methods

Fifteen subjects were investigated using 3T MRI (Philips Achieva). For estimation of absolute CBV values, T1 measurements (for the Bookend technique) and VASO experiments were performed before and after a DSC-MRI experiment with administration of 0.1 mmol/kg b.w. contrast agent. Arterial spin labelling (ASL) was performed before the other measurements. The calibration factors were obtained by comparing CBV values from Bookend and VASO with DSC-MRI CBV values in the same region. Calibration factors were estimated from both white and grey matter regions and both CBV and CBF maps from DSC-MRI were calibrated using the retrieved calibration factors. Grey-matter CBF values in calibrated DSC-MRI images were compared to the corresponding values from ASL.

Results

The mean value of CBF in grey matter obtained by DSC-MRI was 313 ml/(min 100 g) before any calibration. After applying calibration factors from Bookend, the mean value reduced to 33 ml/(min 100 g) and 29 ml/(min 100 g) using calibration factors from grey and white matter, respectively. Calibration factors obtained from VASO resulted in mean values of 42 ml/(min 100 g) and 38 ml/(min 100 g) using calibration factors based on grey and white matter, respectively. These estimates can be compared to the ASL-based mean CBF value of 44 ml/(min 100 g). The correlation between CBF estimates in grey matter obtained by DSC-MRI and ASL was improved when calibration factors from Bookend were used and when grey-matter based calibration factors from VASO were applied.

Conclusion

Bookend and VASO techniques can be used for calibration of CBV and CBF estimates from DSC-MRI. The values obtained after calibration were more reasonable and the correlation with ASL improved for most of the calibration factors used. However, there is a need for further investigation of the methods, including optimization of the calibration procedure and validation of the methods against other perfusion modalities.

Abbreviations

aBV	Arterial blood volume
AIF	Arterial input function
ASL	Arterial spin labelling
CA	Contrast agent
CBF	Cerebral blood flow
CBV	Cerebral blood volume
CF	Correction factor
CT	Computed tomography
DSC	Dynamic susceptibility contrast
EPI	Echo planar imaging
FOV	Field of view
GM	Grey matter
MRI	Magnetic resonance imaging
MTT	Mean transit time
TI	Inversion time
ROI	Region of interest
SENSE	Sensitive encoding
SNR	Signal to noise ratio
SPECT	Single photon emission computed tomography
PET	Positron emission tomography
QUASAR	Quantitative signal targeting with alternating radiofrequency labelling of arterial regions
TC	Cycle time
TE	Echo time
TFE	Turbo field echo
TR	Repetition time
VASO	Vascular space occupancy
WM	White matter

Table of Contents

Part of this work has been accepted for oral presentation at the 26th Annual Meeting of the European Society for Magnetic Resonance in Medicine and Biology (ESMRMB), October 1-3, 2009, Antalya, Turkey.

Introduction

The term perfusion refers to the tissue capillary blood flow. Since nutrition and oxygen are transported by the blood and delivered to the tissue at the capillary level, the perfusion is often a good measure of tissue viability. Assessment of perfusion in the brain can be of interest for investigation of several neurological diseases such as acute ischemic stroke [1-3], tumour in the central nervous system [4, 5], dementia (including Alzheimer's disease) [6, 7], epilepsy [8] and depressive disorders [9, 10].

Brain perfusion is also denoted cerebral blood flow (CBF) and is typically expressed in ml/(min 100 g). Other haemodynamic parameters related to the perfusion are the cerebral blood volume (CBV) and the mean transit time (MTT). CBV is usually expressed in ml/(100 g) but can also be expressed as a volume fraction of the voxel that is occupied by blood, giving a dimensionless quantity, and the mean transit time (MTT) is expressed in seconds.

Arterial spin labelling (ASL) and dynamic susceptibility contrast MRI (DSC-MRI) are two inherently different methods to measure perfusion by MRI. ASL is a non-invasive technique in the sense that no contrast agent (CA) is injected but instead the blood-water protons in a brain-feeding artery are magnetically labelled with a radiofrequency (RF) pulse [11, 12]. CBF can, in principle, be measured by ASL, while CBV and MTT are inaccessible. This makes ASL unsuitable, for example, for assessment of the effects of autoregulation. In DSC-MRI, a CA (usually gadolinium based) is injected and the first passage through the brain is monitored by rapid T2*-weighted imaging [13-15]. DSC-MRI provides maps of all the three parameters CBF, CBV and MTT. The absolute values of CBV and CBF are often overestimated due to methodological problems associated with the technique but the relative values seem reasonably correct, with typical grey-to-white matter ratios of around 2-3 [16].

Perfusion can also be measured with other imaging modalities such as positron emission tomography (PET), single photon emission computed tomography (SPECT) and computed tomography (CT). Examination with PET is often regarded to be the gold-standard method but the need of a cyclotron limits its clinical availability and the images provided by PET measurements have relatively low spatial resolution. PET, SPECT and CT involve ionizing radiation which is a substantial disadvantage when sequential measurements are required and in the examination of small children.

There are several reasons why it is of considerable interest to quantify CBF, CBV and MTT in absolute terms. The absolute values make it possible to compare results between different subjects and also between examinations of the same subject at different points in time, for example, during the course of treatment. The absolute values are also of great interest for detailed investigation of several diseases. One example is for patients with ischemic stroke. During the first hours after the occurrence of stroke, the patient can be treated with chemical thrombolysis. However, such treatment increases the risk of haemorrhage and it has been shown that the value of CBF may be a good indicator of whether the treatment will be successful or not [17]. It has also been proposed that the combination of perfusion and diffusion images may be able to show the so-called ischaemic penumbra region which is the region that is treatable and potentially salvageable [1, 2]. The hypothesis is that perfusion images show both the region that is untreatable and the region at risk of being further damaged within the next hours or days. The diffusion images are assumed to show only the

tissue that is untreatable, and the difference or mismatch between perfusion and diffusion information thus shows the tissue that can be saved with appropriate treatment. If this region is large, there are good reasons for treatment with thrombolysis if one is willing to accept the risk of haemorrhage. If the mismatch region is small or absent, the risk for haemorrhage may be regarded as unacceptable because the chance of saving tissue is small. Recent studies on the prediction of final infarct have, however, indicated that this issue is more complex. A study from 2009 with 82 patients with probable or definite stroke showed no relationship between the mismatch of perfusion and diffusion images and the functional outcome after the stroke [18]. However, by including additional parameters such as the oxygen supply of the tissue when studying the perfusion-diffusion mismatch, the prediction of tissue at risk can be improved [19].

Quantification of perfusion-related parameters can also be useful in investigations of patients with tumours in the central nervous system. The values of CBV can be used to classify the malignancy grade of the tumour since CBV tends to increase with increasing malignancy [4]. This is related to the angiogenesis, i.e. the creation of new vessels surrounding the tumour. It is also possible to monitor the effects of the treatment of a tumour by CBV measurements. If the treatment is successful, CBV tends to decrease in the tumour region [5].

Vascular dementia is another disease that can be investigated using perfusion measurements. Patients with vascular dementia have reduced blood supply to the brain which leads to reduced CBV [6, 7]. A global perfusion reduction is also observed in patients who suffer from depressive disorders, and quantification of perfusion can be of importance to diagnose these patients [9, 10].

Different approaches have been proposed to accomplish absolute quantification of perfusion parameters by MRI. Measurement with ASL provides CBF values that seem reasonable, at least in grey matter, but the images are often noisy and, as pointed out above, CBV and MTT can not be obtained. DSC-MRI seems to suffer from a proportional error in CBV and CBF estimates [20] originating from inherent problems with the technique, particularly related to accurate registration of the arterial input function (AIF) and its time integral. One potential way to improve quantification of DSC-MRI data would be to use a correction factor for the CBF and/or the CBV maps from DSC-MRI measurement. Both population-based and patient-specific correction factors have been proposed, but it has been shown that a patient-specific correction factor tends to give better agreement with values from measurements with PET [21].

In this work, two ways of calibrating the DSC-MRI data were implemented and the results were compared with the corresponding CBF results from ASL. The DSC-MRI measurement was calibrated with values from T_1-based steady-state CBV measurements (the so-called Bookend approach [22, 23]) and the vascular space occupancy (VASO) method [24]. In the Bookend method, the difference in T_1 before and after contrast-agent injection in tissue compared to the T_1 difference in blood is extracted, and this provides a measure of the CBV. The CBV is also obtained by the VASO method by using a sequence that nulls the blood before contrast-agent injection. The difference in signal before and after injection of CA is recorded and CBV can be estimated. A patient-specific correction factor is provided when comparing CBV values from Bookend and VASO with the corresponding CBV values from DSC-MRI.

Material and Methods

Theory

Basic calibration approach

The perfusion-related parameters CBV, CBF and MTT can, in principle, be estimated by dynamic susceptibility contrast MRI. The central volume theorem provides the connection between these three parameters [25, 26] :

$$CBV = CBF \cdot MTT \tag{1}$$

Provided that MTT is correctly measured, CBV and CBF can thus be calibrated using the same correction factor (CF). In this study, a subject-specific correction factor for CBV and CBF is determined using steady-state measurement of CBV (CBV_{SS}). The correction factor is determined according to

$$CF = \frac{CBV_{SS}}{CBV_{DSC}} \tag{2}$$

The estimates of CBV_{SS} were acquired using two independent techniques, i.e. a T1-based steady-state approach, called the Bookend method, and a technique based on a blood-nulling pulse sequence called VASO, both techniques further described below.

Dynamic susceptibility contrast MRI

In DSC-MRI, a conventional gadolinium-based CA is injected as a bolus and is tracked using rapid susceptibility-weighted imaging. Since the T_2^* relaxation rate $\Delta R_2^* = 1/\Delta T_2^*$ is assumed to be proportional to the concentration of CA [27], the signal after contrast-agent administration can be expressed as [28]

$$S_C(t) = S_0 e^{-TE \cdot \Delta R_2^*(t)} = S_0 e^{-TE \cdot kC(t)} \tag{3}$$

where $S_C(t)$ is the signal after contrast-agent administration, S_0 is the signal before CA and TE is the echo time. C is the concentration of CA and k is an unknown proportionality constant assumed, as a first approximation, to be equal for artery and tissue. Equation 3 can be rewritten as

$$C(t) = -\frac{1}{k \cdot TE} \ln\left(\frac{S_C(t)}{S_0}\right) \tag{4}$$

By measuring the signal $S_C(t)$ during the passage of CA, the concentration of CA can then be calculated.

The tissue impulse residue function, R(t), describes the fraction of CA that remains in the tissue at time t after the arrival of an infinitely short bolus and can be expressed as [25]

$$R(t) = 1 - \int_0^t h(t)dt \tag{5}$$

where h(t) is the transit-time distribution and $h(t)dt$ is the fraction of CA that leaves the capillary system on the venous side during the time interval t+dt. At t=0 the residual function is equal to one. This assumes a true or ideal bolus injection, but in practice the CA is injected during an extended time and the transport of the CA from the injection site, through the vasculature to the brain also contributes to a bolus that is extended in time. This means that the concentration curve measured in the brain is not ideal and does not reflect an infinitely short arterial bolus. The measured concentration curve in tissue is instead a convolution of the kernel $CBF \cdot R(t)$ and the concentration curve in an artery that supplies the brain tissue of interest, called the arterial input function (AIF) [15, 29]:

$$k_H C(t) = CBF \cdot R(t) \otimes AIF(t) = CBF \int_0^t AIF(\tau) R(t-\tau) d\tau \tag{6}$$

$CBF \cdot R(t)$ can consequently be obtained by deconvolution of the measured concentration curve C(t) and the AIF. Since R(0)=1, CBF can be obtained as the initial height on the $CBF \cdot R(t)$ curve. The constant k_H takes into account the different densities in brain tissue and blood and also corrects for the fact that the haematocrit levels in large and small vessels differ (which is relevant because a plasma tracer is used). The haematocrit is the volume fraction of red blood cells in the blood.

$$k_H = \frac{1}{\rho} \cdot \frac{1 - H_{LV}}{1 - H_{SV}} \tag{7}$$

where ρ is the brain density and H_{LV} and H_{SV} are the hematocrit values in large and small vessels, respectively. In this study a k_H value of 0.705 was used [15] (ρ =1.04 g/ml, H_{LV} =0.45 and H_{SV}= 0.25).

The relationship between MTT and the tissue impulse residue function is given by Eq. 8 [25]:

$$MTT = \int_0^\infty R(t) dt \tag{8}$$

CBV can be described as an function of C(t) and AIF(t) by combining Eq.1, 6 and 8 in the following way. Integration of Eq. 6 gives the following expression

$$k_H \int_0^\infty C(t) dt = CBF \cdot \int_0^\infty R(t) \otimes AIF(t) = CBF \cdot \left(\int_0^\infty R(t) dt \right) \cdot \left(\int_0^\infty AIF(t) dt \right) \tag{9}$$

Eq. 9 can be expressed as

$$k_H \frac{\int_0^\infty C(t) dt}{\int_0^\infty AIF(t) dt} = CBF \cdot \int_0^\infty R(t) dt \tag{10}$$

As given by Eq. 1, $CBV = CBF \cdot MTT$. Eq. 10 can then be expressed as

$$k_H \frac{\int_0^\infty C(t)dt}{\int_0^\infty AIF(t)dt} = CBF \cdot MTT = CBV \tag{11}$$

and is usually written as

$$CBV = \frac{1}{\rho} \cdot \frac{(1 - H_{LV}) \cdot \int_0^\infty C(t)dt}{(1 - H_{SV}) \cdot \int_0^\infty AIF(t)dt} \tag{12}$$

Many discrete deconvolution algorithms tend to underestimate the initial point of the tissue residue function R(t), especially at short MTTs, and a well-established approach is to use max[R(t)] as an approximation to the true R(0) value [13, 15]. It is thus convenient to express MTT in terms of the Zierler area-to-height relation [30] in practical cases:

$$MTT = \frac{\int_0^\infty R(t)dt}{\max[R(t)]} \tag{13}$$

Overestimation of CBV and CBF

When DSC-MRI is employed, CBV and CBF are often overestimated when the theory outlined above is utilized. This is believed to mainly result from an underestimation of the AIF time integral (i.e. the area under the AIF curve). Two examples of reasons for underestimated AIF time integrals are partial volume effects [31, 32] and different effective relaxivities in tissue and artery [33].

Accurate measurement of the AIF requires a voxel with pure blood, but due to the limited spatial resolution a voxel including both blood and tissue is often inadvertently used in the practical case. Since the CA can be assumed to remain in the blood compartment, the concentration of CA in a voxel containing both blood and tissue is lower than the concentration in a voxel with pure blood, and underestimation of the concentration leads to an underestimated AIF time integral. [31, 32]. The degree to which partial volume effects influence the shape and amplitude of the AIF depends on the orientation of the vessel relative the direction of the main magnetic field. For example, the amplitude of an AIF selected inside the vessel becomes more dependent on the amount of partial volume if the vessel is oriented parallel to the main magnetic field than if the vessel is perpendicular to the main magnetic field. The amplitude and shape of an AIF taken from a voxel close to a vessel can vary considerably depending on the position of the voxel [34].

Another reason for underestimating the AIF is that in the calculation of contrast-agent concentration (cf Eq. 4), it is assumed that the T2* relaxivity, which is the transverse relaxation-rate change induced by the CA at a given concentration, is the same in tissue and in large vessels. In fact, it appears more likely that the relaxivity in a large vessel is lower than

the relaxivity in tissue. This means that the signal change at a given concentration of CA is less in a large vessel than in a tissue environment which will lead to an underestimation of the AIF [33].

Local geometric distortion during the bolus passage can also result in disturbed AIF shapes and an underestimation of the AIF. The distortion is due to the low bandwidth in the phase-encoding direction using single-shot echo-planar imaging (EPI). The high concentration of paramagnetic CA in large vessels causes a shift in frequency of the signal which leads to a local distortion of the image at peak concentration [35].

In the artery there is also a risk that the signal decreases to the level of the background noise during the CA passage. In this case, the full signal drop cannot be registered and the concentration of CA will be correspondingly underestimated (cf. Eq. 4) leading to an underestimation of the AIF [36].

Arterial spin labelling

Arterial spin labelling (ASL) is a non-invasive perfusion-measuring method. Instead of using a gadolinium-based CA, the blood is tagged with an inversion (or saturation) RF pulse applied to the arterial blood on the way to the slice of interest. After a delay, during which the tagged blood reaches the image slice, the magnetization is measured. A control image is also acquired, with no labelling of the blood. The magnetization difference between the two images is proportional to the perfusion, since the difference is only dependent on the amount of tagged blood that entered the imaging slice. Because the difference between the images is very small, repeated measurements and averaging of the images are required to get an acceptable signal-to-noise-ratio (SNR).

The difference between the magnetization levels in the labelled and control images can be expressed as [37]

$$\Delta M(t) = 2 \cdot M_{a,0} \cdot CBF \cdot \int_0^t c(\tau) \cdot r(t-\tau) \cdot m(t-\tau) d\tau \qquad (14)$$

where $M_{a,0}$ is the equilibrium magnetization in blood, $c(\tau)$ is the fractional arterial input function, $r(t-\tau)$ is the fractional residue function, meaning the fraction of the labelled spins that arrived at a voxel at time τ that still remain in the voxel at time t. Furthermore, $m(t-\tau)$ is the magnetization relaxation term describing the longitudinal magnetization fraction of the labelled spins that arrived at a voxel at time τ that still remain in the voxel at time t.

It is common that a standard model for quantification, based on an assumption of plug flow, is used. However, a deconvolution-based, model-free approach for quantification of CBF, dubbed quantitative signal targeting with alternating radiofrequency labelling of arterial regions (QUASAR), has been presented by Petersen et al. [38]. Using this method, images are acquired at different inversion times after labelling, allowing the entire signal difference curve over time to be obtained and thereby minimizing errors that can be present when images at a single inversion time point are acquired, for example, in patients with a wide transit-time distribution. Also, using this method, ASL images are obtained with crushed arterial signal, using a velocity-encoding gradient (crushed data), as well as with retained arterial signal (non-crushed data). The fractional AIF $c(\tau)$ can then be derived by subtracting the crushed data from the non-crushed data and the AIF can be calculated according to:

$$AIF(\tau) = 2 \cdot M_{a,0} \cdot c(\tau) . \qquad (15)$$

The residue function can be expressed as

$$R(t-\tau) = r(t-\tau) \cdot m(t-\tau). \tag{16}$$

A combination of equations 14, 15 and 16 gives the expression [38]

$$\Delta M(t) = CBF \cdot \int_0^t AIF(\tau) \cdot R(t-\tau) d\tau. \tag{17}$$

Since ΔM(t) and AIF(τ) can be measured, CBF can be obtained after deconvolution according to Eq 17.

The arterial blood volume (aBV) can be calculated according to:

$$aBV = \frac{\int_{-\infty}^{\infty} \left(\Delta M_{ncr}(t) - \Delta M_{cr}(t)\right) e^{\frac{t}{T_{1,a}}} dt}{2 \cdot M_{a,0} \cdot \tau_b \cdot \alpha} \tag{18}$$

where $T_{1,a}$ is the longitudinal relaxation time of the blood, τ_b is the duration of the labelling of the blood and α is the inversion efficiency. ΔM_{cr} and ΔM_{ncr} are the crushed and non-crushed data, respectively.

Vascular space occupancy (VASO)

By using a non-slice-selective inversion pulse with an inversion time that nulls the signal from blood before contrast-agent administration, and by comparing the signal before and after contrast-agent administration, CBV can be estimated [24]. This method is called vascular space occupancy (VASO). The repetition time used is quite long (about 6 s) and the echo time is short (about 6 ms). Imaging with the same sequence is performed before and after injection of CA and the signal before CA in a voxel with CBV fraction of blood and 1-CBV fraction of tissue can then be described using the following equation [24]:

$$S_{pre} = S_{tissue} + S_{blood} = A \cdot \left[\left(C_{par} - CBV \cdot C_b\right) \cdot \left(1 - 2 \cdot e^{-TI/T_{1,t}}\right) + 0\right] \tag{19}$$

The constant A gives the MR signal per unit volume of water protons when the tissue is at equilibrium, C_{par} is the water proton density of parenchyma and C_b is the water proton density of blood. TI is the inversion time and $T_{1,t}$ is the longitudinal relaxation time in tissue.

The signal from blood in the image before the injection of CA is null because of the appropriately selected inversion time. With the long repetition time, the tissue magnetization is at equilibrium before the inversion pulse, giving the expression $1 - 2 \cdot e^{-TI/T_{1,t}}$. Since the echo time is short, the term describing the transverse magnetization can be excluded from the expression for the signal in Eq. 19.

After injection of CA the longitudinal relaxation time (T_1) in blood decreases. Imaging with the same parameters as before the contrast-agent administration then leads to a non-zero

signal. The signal after contrast-agent administration from a voxel with CBV fraction of blood and 1-CBV fraction of tissue can then be described as

$$S_{post} = S_{tissue} + S_{blood} = A \cdot \left[\left(C_{par} - CBV \cdot C_b \right) \cdot \left(1 - 2 \cdot e^{-TI / T_{1,t}} \right) + CBV \cdot C_b \cdot \left(1 - 2 \cdot e^{-TI / T_{1,b,post}} \right) \right] \quad (20)$$

where $T_{1,b,post}$ is the T1 in the blood after contrast-agent administration.

The first term in Eq. 20 is the same as in Eq. 19, and the only difference is due to the change in signal from the blood. This means that the difference between the signal levels before and after the injection of CA is proportional to the blood volume [24].

$$\Delta S = \left| S_{post} - S_{pre} \right| = \left| A \cdot CBV \cdot C_b \left(1 - 2 \cdot e^{-TI / T_{1,b,post}} \right) \right| \quad (21)$$

If $T_{1,b,post}$ is short, the term $e^{-TI / T_{1,b,post}}$ vanishes and it is possible to simplify the expression in Eq. 21 to the following:

$$\Delta S = A \cdot CBV \cdot C_b . \quad (22)$$

This provides a simple way of expressing CBV. When the factor $100 \cdot \frac{1}{\rho}$ is applied, CBV is given in ml/100 g, i.e.

$$CBV = 100 \cdot \frac{1}{\rho} \cdot \frac{\Delta S}{A \cdot C_b} \quad (23)$$

The constant $A \cdot C_b$ can be obtained in a voxel with pure blood in the VASO images acquired after CA administration [24]. Another alternative is to obtain A from a voxel with pure CSF in an image taken with long repetition time and short echo time. The constant C_b describes the water content in blood and is known to be 0.87 ml of water/ml of blood [39].

In Eq. 21, the absolute value is used to practically accommodate cases when the signal after contrast-agent administration has not increased in the modulus data due to partial volume effects [24]. This can be the case in a voxel with tissue, blood and CSF. The magnetization in this case is negative but in the modulus data, i.e. the absolute value of the signal, the signal becomes positive. The signal after contrast-agent administration is indeed higher (less negative) due to additional signal from blood, but in modulus data the signal appears smaller than the signal observed before the CA was provided. Figures 1 and 2 show the modulus signal before and after CA and Figure 3 shows the modulus data in a voxel with tissue, CSF and blood before and after contrast-agent administration. As can bee seen, the signal is lower after contrast-agent administration in the first region of the curve because of the use of modulus data.

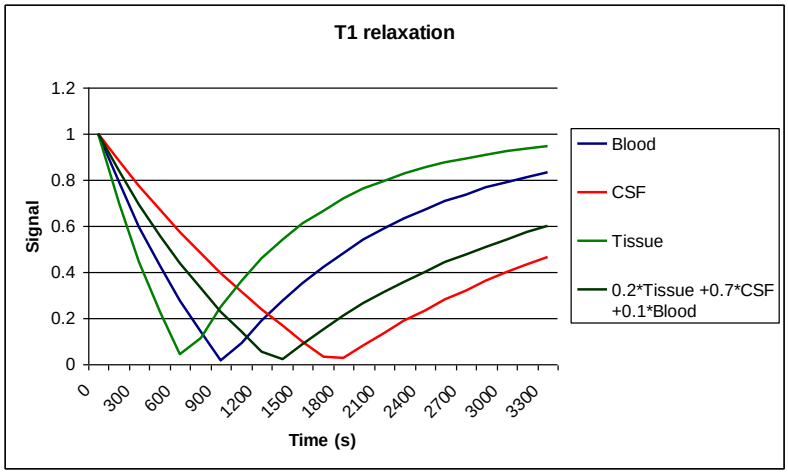

Figure 1. Modulus signal effects due to T1 relaxation before contrast-agent administration in blood, CSF, tissue and a voxel containing a mixture of tissue, CSF and blood.

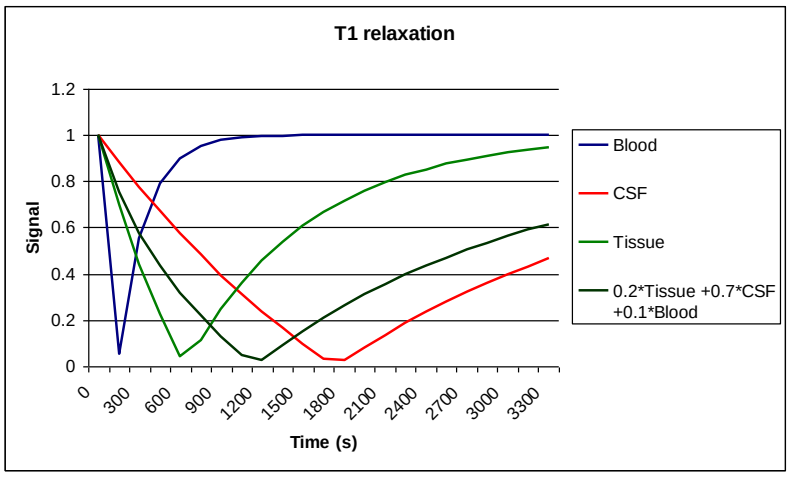

Figure 2. Modulus signal effects due to T1 relaxation after contrast-agent administration in blood, CSF, tissue and a voxel containing a mixture of tissue, CSF and blood.

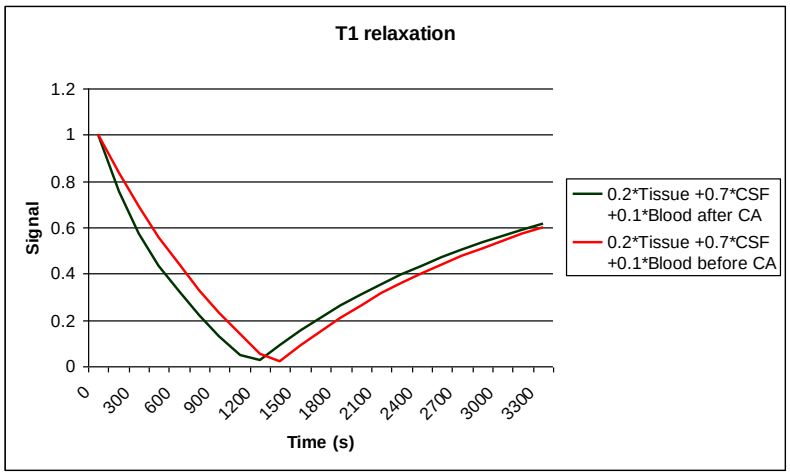

Figure 3. Modulus signal effects due to T1 relaxation before and after contrast-agent (CA) administration in a voxel containing a mixture of tissue, CSF and blood.

Bookend

CBV can also be estimated using T1 values from measurements before and after (at steady-state concentration) contrast-agent administration and this is called the Bookend method [22, 23]. The steady-state longitudinal relaxation rate after contrast-agent administration is given by

$$\frac{1}{T_1^{post}} = r_1 \cdot C + \frac{1}{T_1^{pre}}. \tag{24}$$

where $1/T_1^{post}$ is the longitudinal relaxation rate after contrast-agent injection, at steady-state concentration, $1/T_1^{pre}$ is the longitudinal relaxation rate before contrast-agent injection, r_1 is the longitudinal relaxivity of the CA and C is the concentration of CA. According to Eq. 24, the difference in relaxation rate before and after contrast-agent administration is proportional to the concentration of CA. By studying the difference in relaxation rate in tissue before and after contrast-agent administration compared with the corresponding difference in the relaxation rate in blood, the CBV can be estimated. CBV can be expressed as [22, 23]

$$CBV = 100 \cdot WCF \cdot \frac{1}{\rho} \cdot \frac{1-H_{LV}}{1-H_{SV}} \cdot \frac{\left(1/T_1^{post} - 1/T_1^{pre}\right)_{tissue}}{\left(1/T_1^{post} - 1/T_1^{pre}\right)_{blood}}. \tag{25}$$

H_{LV} and H_{SV} are, as above, the haematocrit levels in large and small vessels, respectively. WCF is a water correction factor by which the water exchange between the intra- and extravascular spaces is taken into account. Under the assumption of an intact blood-brain-barrier the employed CA can be assumed to remain in the intravascular space. However, water in the intravascular space, which has been affected by the CA, may exchange with water in the extravascular space causing T1 to change in the tissue surrounding the blood vessels even though the CA remains in the intravascular space. Simulations have been performed for the two limiting cases no water exchange and fast water exchange [23]. The simulations indicated that the fast-water-exchange limit is the most appropriate but with the need for a water correction factor. The WCF depends on the relaxation-rate change in blood, $dR_{1,blood}$ in s^{-1}, and the magnetic field strength [22, 23]:

$$WCF(dR_{1,blood}) = 8.2 \cdot 10^{-3} dR_{1,blood}^2 + 0.25 \cdot dR_{1,blood} + 0.51 \quad \text{(at 1.5 T)} \tag{26}$$

$$WCF(dR_{1,blood}) = 9.5 \cdot 10^{-3} dR_{1,blood}^2 + 0.30 \cdot dR_{1,blood} + 0.52 \quad \text{(at 3.0 T)} \tag{27}$$

The Bookend method requires a good way to measure the T1 relaxation time. This can be accomplished by different approaches, and in this study a method called QRAPTEST [40] was used. The QRAPTEST is similar to a Look-Locker readout, i.e. a sequence with an inversion pulse followed by a train of turbo field echo (TFE) shots. The signal intensity is measured at different times after the inversion time (in a cycle time, TC) when the signal intensity is increasing due to T1 relaxation and from this signal curve the T1 relaxation time can be estimated. The difference between the original Look-Locker concept and QRAPTEST is that in QRAPTEST there is no time between the TCs and the inversion pulse is replaced by a saturation pulse. The signal intensity at the end of the cycle time M_0^{**} can then be expressed as

$$M_0^{**} = M_0^* \frac{1 - e^{-TC/T_1^*}}{1 - e^{-TC/T_1^*}\cos(\theta)} \tag{28}$$

where M_0^* is the steady-state magnetization and T_1^* is the relaxation time corresponding to the signal-intensity decay and θ is the flip angle of the saturation pulse.

The actual relaxation time T_1 can be estimated if T_1^* is known using the equation

$$\frac{1}{T_1} = \frac{1}{T_1^*} + \frac{\ln(\cos\alpha)}{TR} \tag{29}$$

where α is the flip angle in the TFE and TR is the repetition time.

Experiments

The study included 15 subjects (10 women and 5 men, mean age 48 years, age range 28-67 years) with brain tumour of different types. One subject was excluded from the ASL examination due to extensive motion artefacts, one subject was excluded from the Bookend T1 measurement due to technical problems and one subject had to be excluded from the study due to a large and non-correctable shift in the position of the head between the pre- and post-contrast-agent experiments. The examinations were performed on a 3 T Philips Achieva MRI unit using an eight-channel head coil. The T1 and VASO experiments were performed before as well as after administration of 0.1 mmol/kg bodyweight gadolinium-based CA (Dotarem, Guerbet, Paris, France) and the DSC-MRI experiment was applied to monitor the first passage of the CA through the brain. The CA was injected at a rate of 5 ml/s and followed by a saline flush. The ASL measurement was performed during the same session, before contrast-agent administration. The study was approved by the local ethics committee and written informed consent was provided from all subjects.

The ASL experiment was performed using QUASAR. As mentioned above, this sequence includes collection of crushed and non-crushed data. For destruction of arterial signal, crushed data were obtained using a velocity-encoding gradient corresponding to Venc=[4 cm/s]. Two different flip angles were used in order to measure the equilibrium magnetization in blood. The parameters used for the QUASAR experiment were repetition time 4000 ms, echo time 23 ms, ΔTI 300 ms and TI_1 40 s. The matrix was 64×64 and seven slices with thickness 6 mm and 2 mm slice gap were acquired. The FOV was 240×240 mm^2 and the flip angles were 35° and 11.7°. The SENSE factor used was 2.5.

DSC-MRI was performed using a single-shot gradient-echo EPI with repetition time 1360 ms, echo time 29 ms and flip angle 90°. The slice thickness was 5 mm, with 1 mm slice gap, and 23 slices were acquired. The FOV was 220×220 mm^2 and the matrix size was 128×128. The SENSE factor used was 2.5.

The VASO experiment was performed with a non-slice-selective inversion-recovery sequence with inversion time 1088 ms, repetition time 6000 ms, echo time 5.8 ms, and flip angle 90°. Ten slices with thickness 5 mm and no slice gap were acquired. The FOV was 230×230 mm^2 and the matrix size was 128×128.

The T1 measurements for the Bookend method were performed using a saturation-recovery TFE EPI sequence with flip angle 4°, repetition time 9.6 ms, echo time 4.4 ms and saturation-recovery time 3000 ms. The slice thickness was 5 mm without any slice gap, and 25 slices were acquired. The FOV was 260×260 mm^2 and the matrix size was 288×288.

Post-processing of data

DSC-MRI

CBF maps were calculated using a locally developed computer program (LUPE, Interactive Data Language, IDL 6.0, Research Systems inc Boulder, CO, USA) according to Eq. 6 in the theory section using a block-circulant singular value decomposition (SVD) deconvolution algorithm [41, 42]. A global AIF was employed, obtained from middle cerebral artery (MCA) branches in the Sylvian-fissure region. The AIF was chosen in a semi-automatic way with the criteria that the included concentration curves should be smooth (i.e. not showing any distortion at peak concentration), the baseline signal should be at least 60% of the maximum baseline signal in the investigated volume (since a high baseline signal indicates a voxel containing blood) and the signal value at the maximum signal drop should be below 20 % of the baseline signal. The signal curve after the peak concentration had to return to at least 80% of the baseline signal level and the maximum signal drop had to occur within 2 time points (in this case 2600 ms) after the signal curve showing the earliest maximum signal drop. The identified arterial concentration curves were visually inspected and the mean value of arterial concentration curves from 4-8 pixels was used to create one global AIF.

ASL

Post-processing of the ASL data was performed using a computer program developed by one of the inventors of QUASAR (Dr Esben T Petersen). Pairs of images showing strong motion artefacts were automatically discarded prior to averaging. Perfusion maps were calculated using Eq. 14 in the theory section. The deconvolution was performed using a block-circulant SVD method [41] with an oscillation index of 0.12. The AIFs used for calculation of CBF corresponded to voxels with aBV above a threshold of 1.2% [38].

VASO

CBV was calculated using the expression in Eq. 23. The constant $A \cdot C_b$ was determined as the maximum signal intensity in blood in the posterior sagittal sinus in the post-contrast image, since after the injection of CA the T1 for blood is shorter than for tissue and CSF. This means that a high signal value represents a voxel with less partial volume effects likely to be a voxel with pure blood. The constant A was also determined from an image with long repetition time and short TE in a voxel with pure CSF. The highest signal intensity was chosen also in this case.

To obtain accurate measured signal intensities, the pixel values were corrected using the appropriate scaling factors (called scale slope in Philips terminology). These can be found in the DICOM header. A motion correction for the VASO images acquired before and after contrast-agent administration was made using SPM 5 (Statistical Parametric Mapping, www.fil.ion.ucl.ac.uk/spm/).

Ideally, an inversion time that completely nulls the signal from blood in all slices should be used, but since this is not possible to accomplish with a single TI, the preliminary CBV estimates had to be corrected. In this study, the blood was nulled totally in the most superior slice so the correction factors used were 1.00 0.99 0.97 0.95 0.93 0.91 0.89 0.87 0.85 and 0.83 for the following slices from top to bottom [24]. The correction factors were applied because the difference between the signal from blood before and after contrast-agent administration is smaller in slices with inversion times longer than the inversion time that nulls the blood (see Figure 4). This is due to the contrast-agent-induced difference in the longitudinal relaxation time. In the region with inversion times a little bit longer than the inversion time that nulls the signal from blood (indicated by grey colour in Figure 4), the signal from blood before contrast-agent administration increases more than the signal from blood after contrast-agent administration. If an inversion time longer than the ideal inversion time is employed, the difference between the signal from blood before and after CA administration is less than with the ideal inversion time and to correct for this, the difference in signal was divided by the correction factors above [43].

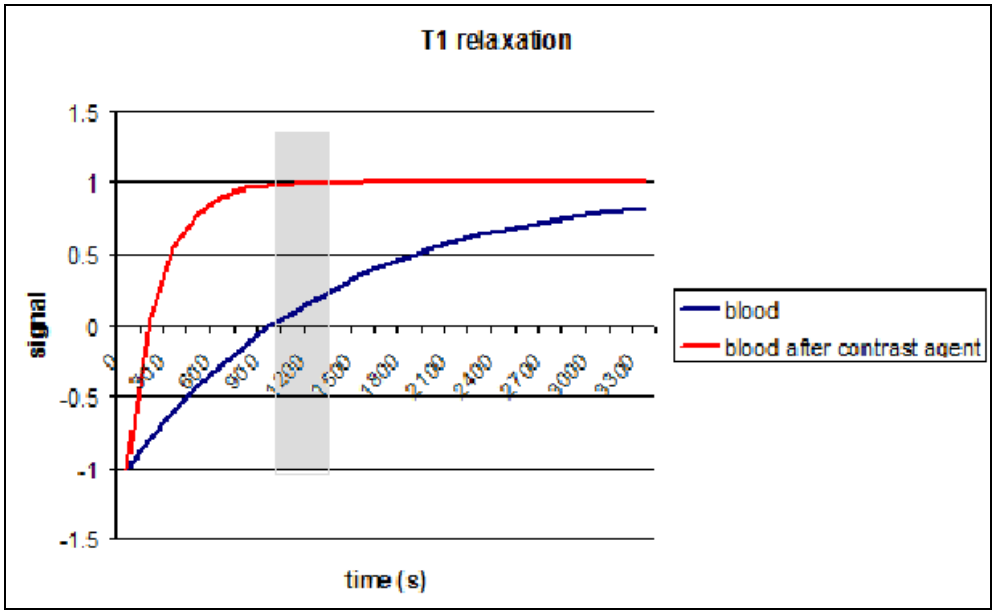

Figure 4. Signal effects due to T1 relaxation for blood before and after contrast-agent administration.

Regions of interest in white matter (WM) and grey matter (GM) were identified using segmentation in regions with no obvious artefacts or pathology, using manually selected threshold pixel values in the VASO images. To avoid inclusion of large vessels in the ROIs, VASO images from the measurements before CA administration were used for the segmentation of white matter while VASO images from measurements post-contrast-agent administration were used for the segmentation of grey matter. White matter has shorter T1 relaxation time than grey matter, and blood has long T1 relaxation time before contrast-agent administration. Hence, the difference in signal between the white matter and the unwanted blood in large vessels is largest before contrast-agent administration. Grey matter has longer T1 relaxation time than white matter, and the segmentation of grey matter was thus done in the post-contrast-agent images, when the T1 relaxation time of blood is shortened, since these images provided the largest signal difference between grey matter and blood in large vessels.

The calibration factor was calculated comparing CBV values from the same regions in the VASO and the DSC-MRI images. The DSC-MRI images were geometrically corrected to

show the same FOV as the VASO images. Since the slice positions in the VASO and DSC-MRI images were not identical, the slices that best corresponded to the volume of interest were selected. Despite the same slice thickness, some of the slices correspond better than others due to the slice gap present in the DSC-MRI images. The slices were aligned manually to correct for patient motion, because SPM motion correction of images from these different perfusion measuring methods turned out to be unreliable due to large differences in contrast and intensity between the different datasets. Regions of interest acquired from the VASO images were applied to the corresponding DSC-MRI CBV map. Pixels in the DSC-MRI CBV map with values above 2.5 times the mean value of all non-zero pixel values in all slices were excluded from the region of interest since these voxels were assumed to correspond to large vessels. The mean values of CBV in white and grey matter in the regions of interests were calculated and the calibration factors were calculated according to Eq. 2.

Bookend

From the T1 measurements, nine or ten images with different TC were obtained. Motion correction of the images before and after CA was performed using SPM. Regions of white and grey matter were identified on the basis of signal values in a high-contrast image, excluding areas with obvious artefacts or pathology. Voxels in the DSC-MRI CBV images that showed values exceeding $2.5 \cdot \text{mean value}$ of the non-zero pixel values in the whole volume were excluded from the region of interest since these voxels were assumed to correspond to large vessels. The mean signal values in the regions of interest were extracted for all different TCs, and the values were plotted as a function of TC. This was done for images acquired before as well as after contrast-agent administration. A curve fit was applied to the values obtained before as well as after contrast-agent injection. Since a 90° saturation pulse was employed, the following function was fitted to the signal values [40]:

$$S = M_0\left(1 - e^{-TC/T1}\right) \tag{30}$$

In the fitting procedure, the constant M_0 was forced to be the same before and after contrast-agent administration. Different values of M_0 were tested, and the M_0 value resulting in the highest sum of r values from the fits before and after contrast-agent administration was selected.

One single pixel within the posterior sagittal sinus was selected to represent blood. The curve fit for T1 estimation in only one pixel was not as stable as the curve fit for a larger region. In this case, a condition was set so that the r value of the curve fit had to be at least 0.95 both before and after contrast-agent administration. The pixel with maximal relaxation-rate difference was chosen as the pixel representing blood. CBV was estimated using Eq. 24 with the values of T1 determined from the curve fit.

For the estimation of the calibration factor, the DSC-MRI images were geometrically corrected so that the FOV corresponded to that of the T1 images. The T1 and DSC-MRI images had the same slice thickness, but in DSC-MRI there was a slice gap between slices. However, the slices in the middle of the volume had the same position and were selected. The selected slices from the two modalities were aligned manually to correct for patient motion (motion correction with SPM was not reliable).

The mean CBV value from the bookend method was compared with the mean CBV value in the corresponding region from the DSC-MRI CBV map, and this provided a correction factor according to Eq. 2.

Evaluation of the results

The calibration factors extracted from the Bookend and VASO measurements were applied to the CBV and CBF maps from the DSC-MRI measurement. Regions of interests were manually identified in white matter (frontal white matter and white matter in one of the most superior slices) as well as grey matter (thalamus, putamen and cortical regions), and mean CBV and CBF values in these white and grey matter regions were calculated for each patient. Figure 5 shows a typical example of the manually identified regions of interest.

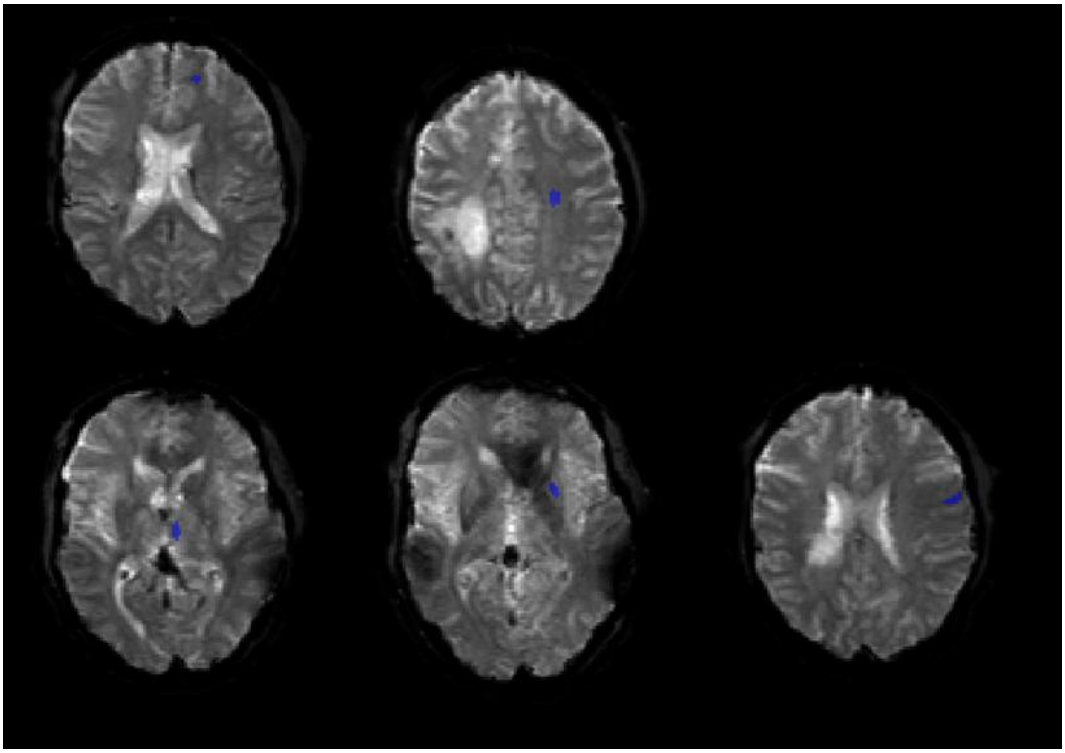

Figure 5. Image showing typical examples of manually identified regions of interest (indicated in blue) in one subject, used for evaluation of the results. The top row shows regions of interest for white matter (left: frontal white matter, right: white matter in one of the most superior slices). The bottom row shows regions of interests for grey matter (left: thalamus, middle: putamen, right: cortical regions).

ASL was used for validation of the absolute values of calibrated CBF in cortical grey matter. No comparison was carried out for white matter because of the noisy and unreliable white-matter estimates typically provided by ASL [44]. To be able to compare CBF values from ASL with the corresponding values from DSC-MRI a given volume must be identified for both modalities. Because different slice thicknesses were used in the DSC-MRI and ASL measurements, the volume of interest was based on three slices from the DSC-MRI images and two ASL slices closely corresponding to the same volume. T1-based masks obtained from the QUASAR experiment were used for visualization of grey-matter regions in order to simplify extraction of grey-matter CBF data from the DSC-MRI and QUASAR maps. A typical example of such a T1-based grey-matter mask obtained from QUASAR is shown in Figure 6.

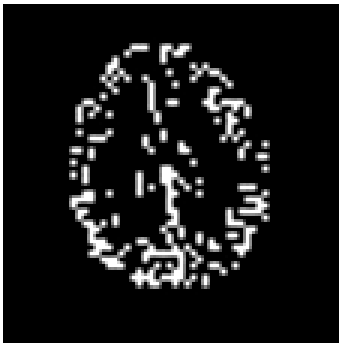

Figure 6. Typical example of a T1-based map obtained from the QUASAR experiment showing grey matter. These images were used for visualization in order to simplify extraction of grey-matter regions.

Statistical analysis of the obtained CBF estimates from calibrated DSC-MRI and ASL was performed using a Wilcoxon signed ranks test.

Results

Figure 7 shows an example of images from the VASO experiment, before and after contrast-agent administration. It also shows the CBVss map calculated according to Eq. 23. Figure 8 shows images before and after contrast-agent administration, used for the Bookend technique. In this case, no CBVss map is shown because Bookend CBVss was only calculated for regions of interest and not pixel by pixel.

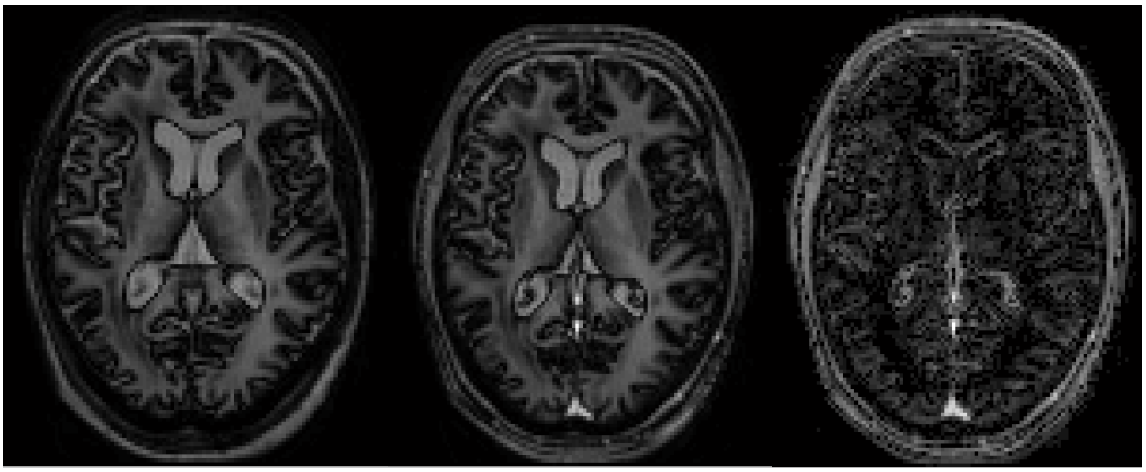

Figure 7. VASO images before and after contrast-agent administration and the corresponding CBVss map.

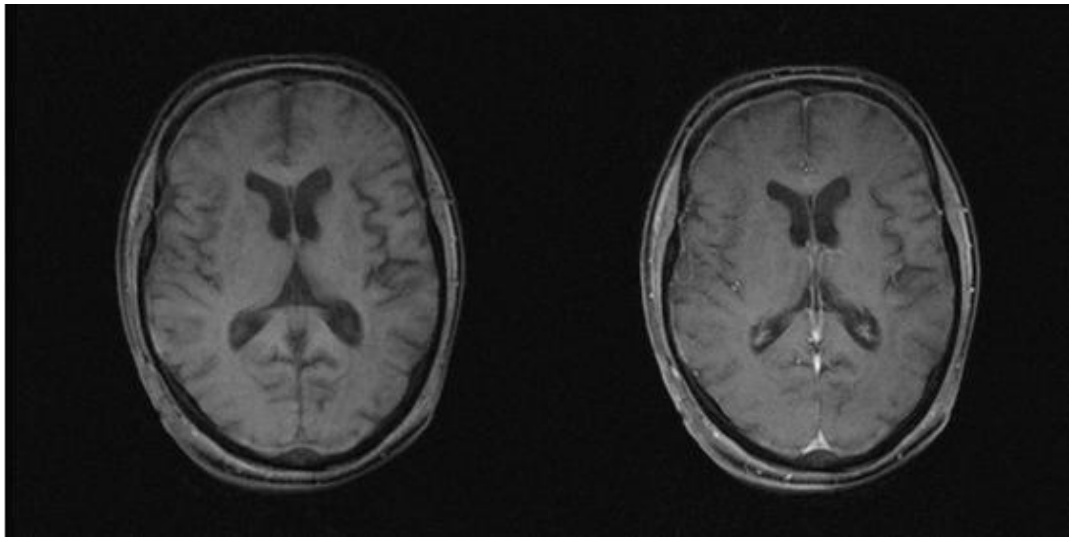

Figure 8. Bookend images before and after contrast-agent administration, from one cycle time, used for the T1 measurement.

The values of CBVss and the subject-specific calibration factors from the Bookend and the VASO methods are provided in Tables A1 and A2 in the Appendix. For the VASO method, the results shown are based on calculations using the constant A as the maximum value from CSF and the constant C_b=0.87 ml of water/ml of blood (in Eq. 23).

Tables A3 to A7 in the Appendix show the calibrated values of CBV and CBF and the original values of MTT from manually selected regions of interests.

Table A8 in the Appendix shows values used for comparison between ASL and DSC-MRI. CBF values from cortical grey matter are obtained by DSC-MRI (non-calibrated as well as calibrated using different calibration factors) and ASL. The values differ between the values in table A6 due to different region of interests. The correlation between DSC-MRI and ASL can be assessed from Figures A1-A5.

The relationship between CBF estimates in cortical grey matter obtained by DSC-MRI and ASL showed a correlation coefficient of 0.52 (p=0.0577) without any calibration of the DSC-MRI images (Figure A1). After calibration with a Bookend calibration factor from white matter, the correlation was improved to 0.56 (p=0.0482) (Figure A2) and with a Bookend calibration factor from grey matter the correlation was 0.63 (p=0.0242) (Figure A3). VASO calibration factors from white matter resulted in a correlation coefficient of 0.45 (p=0.0956) (Figure A4) when comparing DSC-MRI and ASL and for the VASO calibration factor from grey matter the correlation coefficient was 0.57 (p=0.0351) (Figure A5).

Statistical analysis showed that the median difference between ASL and non-calibrated DSC as well as between ASL and DSC calibrated using Bookend was significantly different from zero. (ASL vs non-calibrated DSC: p=0.0001, ASL vs DSC Bookend(WM): p=0.0015, ASL vs DSC Bookend(GM): p=0.0046,). However, when comparing ASL with DSC-MRI calibrated using VASO, the differences were not statistically significant (ASL vs DSC VASO (WM): p=0.1531, ASL vs DSC VASO(GM): p=0.5879). Furthermore, the differences were

not statistically significant when comparing the use of grey and white matter for calibration, neither for Bookend nor for VASO calibration (DSC Bookend(GM) vs DSC Bookend(WM): p=0.2439 , DSC VASO(GM) vs DSC VASO (WM): p=0.2166). The difference between DSC-MRI values obtained by Bookend calibration and by VASO calibration were also statistically significant different from zero (DSC Bookend(GM) vs DSC VASO(GM): p=0.0269, DSC Bookend(WM) vs DSC VASO(WM): p=0.0266).

Figs. A12-A17 in the Appendix show Bland-Altman plots comparing CBF values obtained in grey matter in DSC-MRI images calibrated with GM-based and WM-based calibration factors from Bookend and VASO. The values are also compared to CBF values obtained by ASL. In order for two methods to show good agreement the scatter should be distributed around a mean difference of zero and the lines indicating mean±1.96·SD should be close to the mean difference.

Discussion

With regard to the study population average, DSC-MRI measurements calibrated by both VASO and Bookend CBV estimates provided more reasonable values of CBV and CBF than the non-calibrated DSC-MRI values, but it should be noted that the calibration procedure returned physiologically unreasonable estimates in some cases (cf. Table A3-A5, e.g., subjects 4 and 7). The study population average of CBF values obtained after calibration was much closer to the CBF obtained by ASL than the mean value of the non-calibrated DSC-MRI estimates. However, a Wilcoxon signed ranks test showed that the median of the differences between CBF values from ASL and values from DSC-MRI calibrated with Bookend were significantly different from zero. This means that there is a significant difference between CBF values from these two modalities. The mean CBF values from the DSC-MRI images calibrated with Bookend were all lower than the corresponding ASL-based values. The Bland-Altman plots comparing the Bookend method and ASL showed a clear bias (without any obvious proportional error) and confirmed that the Bookend method provided considerably lower values than ASL. Also compared with $H_2{}^{15}O$ PET and Xe-CT studies, in which observed GM perfusion estimates have typically been in the range 40–60 ml/(min 100g) [45-47], the values were considerably lower. Earlier studies with the Bookend method as a calibration method for DSC-MRI images have also shown rather low values of CBV and CBF. In a study by Shin et al [22], the mean GM value of CBV was 2.93 ml/(100 g) and GM CBF was 47.4 ml/(min 100 g) and values obtained in the present study are even lower. One possible reason for this can be that higher spatial resolution was used in the T1 measurement in the present study. Higher resolution means smaller voxels and thus reduced partial volume effects in the voxel used for pure blood. The difference in longitudinal relaxation rate before and after CA administration then becomes larger, leading to a larger denominator in Eq. 25 and smaller CBV values.

CBV and CBF values obtained from DSC-MRI images calibrated using VASO were higher than the values from Bookend calibration but still a bit lower than literature values. The Bland-Altman plot comparing VASO calibration with ASL showed a positive mean difference without any signs of a proportional error, indicating that the VASO method provided somewhat lower values than the ASL method. However, ASL and DSC-MRI calibrated with VASO provided CBF values in the same range and the Wilcoxon signed ranks test showed that the median of the differences between CBF values from ASL and DSC-MRI

calibrated with VASO was not significantly different from zero. The VASO method has not previously been used to calibrate DSC-MRI but Lu et al. [24] obtained VASO-based CBV values in thalamus grey matter of 3.6 ml blood/100 ml brain which corresponds to approximately 3.5 ml/(100 g), i.e. clearly higher values than in the present study.

The Bland-Altman plots comparing CBF values obtained using the Bookend and VASO calibration approaches showed a negative mean difference indicating that the VASO method provided higher values than the Bookend method, as also pointed out above. No obvious proportional errors could be seen as the scatter was fairly evenly gathered around the mean difference. One reason for the difference between these methods might be that the Bookend approach includes a correction factor to obtain whole-blood volume when a plasma tracer is used. The application of such a correction factor, however, assumes that no water exchange occurs between plasma and red blood cells. In the VASO approach, on the other hand, rapid water exchange between plasma and red blood cells is assumed and no haematocrit correction factor is employed [48]. Hence, the VASO and Bookend methods assume the opposite extreme cases with regard to water exchange between plasma and red blood cells and in future studies it would be interesting to investigate the importance of this phenomenon in the T1 measurement.

The CBVss values, obtained from the Bookend and VASO experiments, used for estimation of the calibration factors were closer to literature values than the CBV values obtained in manually selected regions of interest in the calibrated DSC-MRI images. The lower values compared with gold-standard methods (e.g., PET) imply that the obtained calibration factors were too small. This could be due to problems with matching of the VASO/DSC-MRI and Bookend/DSC-MRI images. It can also be due to the positions of the regions of interest used for estimation of CBV and CBF in the calibrated DSC-MRI images. These regions obviously differ from the calibration factor regions.

The mean values of CBV and CBF in grey matter from calibrated DSC-MRI did not differ much depending on whether the calibration factor was based on regions of interest in white or in grey matter. In theory, since absolute CBV estimation with Bookend and VASO is assumed to be correct and DSC-MRI is assumed to provide accurate CBV values in relative terms, the calibration factor should be independent on the use of white or grey matter regions. The difference between calibration factors based on white and grey matter regions can be due to a matching problem of the VASO/DSC-MRI and Bookend/DSC-MRI images or distortion in the DSC-MRI image. In previous studies, the calibration factor has been obtained in white matter only [22]. Since white matter is found in larger, fairly homogeneous regions, it is easier to identify a large region of interest in white matter. However, since CBV is lower in white matter than in grey matter, the effect of noise is more pronounced and the uncertainty is larger. Calibration factors based on grey matter should then be more accurate. In this study, DSC-MRI images calibrated with calibration factors based on grey matter regions gave better correlation with ASL. Since it is more difficult to identify a region of interest in grey matter the risk of including large vessels and cerebrospinal fluid is larger. If large vessels are included in the region of interest the contrast-agent concentration is high and CBV will be overestimated. However, due to image-matching problems or distortions in the DSC-MRI images, large vessels could be included in these images but not in the images used for CBVss estimation. Even though this is taken into account by not allowing high values in the DSC-MRI images this can be a problem. In this case CBV will be underestimated. Inclusion of cerebrospinal fluid in the regions of interest corresponds to an underestimation of CBV in grey matter since the CA does not reach the cerebrospinal fluid, and this leads to a reduced

effect of the CA. This is the case in voxels with partial volume effects, including both grey matter and cerebrospinal fluid. The motion correction in the feet-to-head direction of the images used for Bookend and VASO can enhance the problem of partial volume effects. The correction is carried out by mixing data from neighbouring slices and creating a new slice by interpolation. The effective slice thickness and the number of pixels with partial volume effects increase and this means that the risk of including pixels with a partial volume effect in the region of interest increases.

For the DSC-MRI versus ASL relationships, the slope of the linear regression equation was lower than one for all calibration factors. This means that the low values in the calibrated DSC-MRI images are overestimated and the high values are underestimated provided that the values of CBF are correct when measured with ASL. The intercept was fairly satisfactory with all calibration factors.

The correlation, intercept and slope results can when put together indicate if there is any agreement between two methods measuring the same parameter. QUASAR has recently been validated against PET and SPECT measurements and the reproducibility of the QUASAR method has been proven to be satisfactory [49-51]. A comparison of the calibrated DSC-MRI CBF images with QUASAR ASL CBF is thus clearly relevant. However, the QUASAR ASL CBF values should not be interpreted as "true CBF" and the obtained values of correlation, intercept and slope should be interpreted with care since both modalities suffer from uncertainties. Because of relatively few subjects, the values from a single subject can have a substantial influence on the degree of correlation. For example, the QUASAR method suffers from low signal-to-noise ratio, limited temporal resolution and artefacts due to head movements of the subject. The fact that there is some degree of correlation between the two methods is, however, promising but further investigations about the accuracy of both the VASO and the Bookend methods are warranted. A reliable comparison requires more subjects to be included. It would also be interesting to assess the reproducibility of the calibration methods and to carry out comparisons with other perfusion-measuring methods such as PET, SPECT and CT.

During the present work, it became clear that the region of interest used for the estimation of the correction factor influenced the value quite markedly. The threshold values applied for segmentation of white and grey matter can change the calibration factor to some extent, and even the region where the segmentation is performed is of relevance. This can partly be due to problems in matching the CBVss images and the DSC-MRI images; the same region of interest is used in the CBVss images as in the DSC-MRI images so correct matching of the images is very important. Furthermore, images from different methods show different contrast and signal so the SPM-based motion correction for Bookend/DSC-MRI images and VASO/DSC-MRI images was suboptimal and automatic motion correction before and after contrast-agent administration could only be accomplished for the Bookend and the VASO methods. Motion correction between the Bookend and DSC-MRI images and the VASO and the DSC-MRI images was made manually after visual inspection. To eliminate this problem, different regions of interest can be manually outlined in the steady-state measurements and in the DSC-MRI images, based on anatomic regions instead of segmentation based on pixel values. In this case, matching of images is not important and it should be more certain that the same kind of tissue is compared. However, it is desirable to use a method where the region of interest is automatically chosen since it reduces the influence of the user.

Other reasons for the differences between calibration factors based on different regions could be noise and distortions in the DSC-MRI images due to the single-shot EPI acquisition. In future studies, it would be interesting to investigate in more detail how much the calibration factors differ between different regions in the brain and the reason for these differences. To get a more accurate result, the calibration factors can be based on the whole brain or from regions of interest in white and grey matter from the whole volume instead of only one slice as was done in this study. However, the regions of interest should not include any pathology. Investigations of this kind can be evaluated by establishing whether changes in the calibration methodology are reflected by an improved correlation with a reference technique (e.g., ASL or PET).

Another future improvement is to calculate the Bookend T1 values more accurately. The change in T1 after contrast-agent administration is very small in tissue so high demands are put on the T1 measurement. Non-optimized parameters (probably too short TR) in the present T1-measurement sequence made it impossible to use the intended software for T1 calculations and T1 had to be estimated according to Eq. 30 instead. In this fitting procedure, $T1^*$ is estimated instead of T1 since the flip angle α is not considered. T1* is shorter than T1 but the flip angle and the TR are supposed to be the same both before and after contrast-agent administration meaning that $T1^*$ is shorter both before and after contrast-agent administration. If α and TR are constant, the difference in longitudinal relaxation rate is most likely not influenced by the use of $T1^*$ instead of T1. A small change in flip angle can, however, influence the relaxation-rate difference and to obtain more accurate results this should be corrected for. In this study, a short TR was used (shorter than recommended for the sequence) and, according to Eq. 29, the difference between T1 and $T1^*$ then becomes larger. A small change in flip angle then leads to a larger error in the calculation of the difference in longitudinal relaxation rate. For estimation of T1*, Eq 28 was simplified by the approximation that the saturation pulse was always 90°. In practice, the uncertainty of the saturation pulse flip angle is about ±3°. If the saturation flip angle is 90° ±3° the estimated T1* value would be 900 ms ± 39 ms for a true T1* value of 900 ms, corresponding to an error of about 4%. Since the change in tissue T1* after CA administration is expected to be in the same range, the flip-angle uncertainty can, in the worst case, have a considerable influence on the result and may, to some extent, have contributed to the unreasonable CBF values seen in some subjects after calibration with the Bookend method.

One considerable problem in both the Bookend and the VASO methods is the need to identify a pixel or a region with pure blood or pure CSF. The risk of partial-volume effects increases, particularly for blood, if a larger number of pixels are used. However, if only one voxel is used to represent blood or CSF, random noise contributions may influence the measured value. This problem is more pronounced for the VASO method since the CSF value is taken from one single voxel in one image. The Bookend method also relies on one voxel to be identified as pure blood, but the T1 value in this voxel is calculated from a number of measurements and this is likely to reduce the effects of noise. In future work, the influence of using the mean value from a larger number of blood and CSF voxels should be investigated.

Conclusion

CBVss measurements using Bookend and VASO methods can be used to calibrate CBV and CBF estimates from DSC-MRI. The values obtained after calibration were more reasonable, but somewhat lower than values reported in the literature. The correlation with ASL was reasonable but depended on from what region calibration data were acquired. More research is needed to optimize the calibration procedure, and validation of the calibration methods against other perfusion modalities would certainly be of interest. The reproducibility of the methods should also be further investigated.

Acknowledgment

We would like to thank Dr Esben Peterson for providing the QUASAR measurement and evaluation package and Dr Marcel Warntjes for providing the QRAPTEST sequence.

References

1. Rordorf G, Koroshetz WJ, Copen WA, Cramer SC, Schaefer PW, Budzik RF, Jr., Schwamm LH, Buonanno F, Sorensen AG, Gonzalez G. Regional ischemia and ischemic injury in patients with acute middle cerebral artery stroke as defined by early diffusion-weighted and perfusion-weighted MRI. Stroke 1998; 29(5): 939-943.
2. Neumann-Haefelin T, Wittsack HJ, Wenserski F, Siebler M, Seitz RJ, Modder U, Freund HJ. Diffusion- and perfusion-weighted MRI. The DWI/PWI mismatch region in acute stroke. Stroke 1999; 30(8): 1591-1597.
3. Wu O, Koroshetz WJ, Ostergaard L, Buonanno FS, Copen WA, Gonzalez RG, Rordorf G, Rosen BR, Schwamm LH, Weisskoff RM, Sorensen AG. Predicting tissue outcome in acute human cerebral ischemia using combined diffusion- and perfusion-weighted MR imaging. Stroke 2001; 32(4): 933-942.
4. Aronen HJ, Gazit IE, Louis DN, Buchbinder BR, Pardo FS, Weisskoff RM, Harsh GR, Cosgrove GR, Halpern EF, Hochberg FH, et al. Cerebral blood volume maps of gliomas: comparison with tumor grade and histologic findings. Radiology 1994; 191(1): 41-51.
5. Wenz F, Rempp K, Hess T, Debus J, Brix G, Engenhart R, Knopp MV, van Kaick G, Wannenmacher M. Effect of radiation on blood volume in low-grade astrocytomas and normal brain tissue: quantification with dynamic susceptibility contrast MR imaging. AJR Am J Roentgenol 1996; 166(1): 187-193.
6. Harris GJ, Lewis RF, Satlin A, English CD, Scott TM, Yurgelun-Todd DA, Renshaw PF. Dynamic susceptibility contrast MR imaging of regional cerebral blood volume in Alzheimer disease: a promising alternative to nuclear medicine. AJNR Am J Neuroradiol 1998; 19(9): 1727-1732.
7. Bozzao A, Floris R, Baviera ME, Apruzzese A, Simonetti G. Diffusion and perfusion MR imaging in cases of Alzheimer's disease: correlations with cortical atrophy and lesion load. AJNR Am J Neuroradiol 2001; 22(6): 1030-1036.
8. Wu RH, Bruening R, Noachtar S, Arnold S, Berchtenbreiter C, Bartenstein P, Drzezga A, Tatsch K, Reiser M. MR measurement of regional relative cerebral blood volume in epilepsy. J Magn Reson Imaging 1999; 9(3): 435-440.
9. Fountoulakis KN, Iacovides A, Gerasimou G, Fotiou F, Ioannidou C, Bascialla F, Grammaticos P, Kaprinis G. The relationship of regional cerebral blood flow with subtypes of major depression. Prog Neuropsychopharmacol Biol Psychiatry 2004; 28(3): 537-546.
10. Ohgami H, Nagayama H, Akiyoshi J, Tsuchiyama K, Komaki S, Takaki H, Mori H. Contributing factors to changes of cerebral blood flow in major depressive disorder. J Affect Disord 2005; 87(1): 57-63.
11. Detre JA, Leigh JS, Williams DS, Koretsky AP. Perfusion imaging. Magn Reson Med 1992; 23(1): 37-45.
12. Williams DS, Detre JA, Leigh JS, Koretsky AP. Magnetic resonance imaging of perfusion using spin inversion of arterial water. Proc Natl Acad Sci U S A 1992; 89(1): 212-216.
13. Ostergaard L, Weisskoff RM, Chesler DA, Gyldensted C, Rosen BR. High resolution measurement of cerebral blood flow using intravascular tracer bolus passages. Part I:

Mathematical approach and statistical analysis. Magn Reson Med 1996; 36(5): 715-725.
14. Ostergaard L, Sorensen AG, Kwong KK, Weisskoff RM, Gyldensted C, Rosen BR. High resolution measurement of cerebral blood flow using intravascular tracer bolus passages. Part II: Experimental comparison and preliminary results. Magn Reson Med 1996; 36(5): 726-736.
15. Rempp KA, Brix G, Wenz F, Becker CR, Guckel F, Lorenz WJ. Quantification of regional cerebral blood flow and volume with dynamic susceptibility contrast-enhanced MR imaging. Radiology 1994; 193(3): 637-641.
16. Kuppusamy K, Lin W, Cizek GR, Haacke EM. In vivo regional cerebral blood volume: quantitative assessment with 3D T1-weighted pre- and postcontrast MR imaging. Radiology 1996; 201(1): 106-112.
17. Lin W, Lee JM, Lee YZ, Vo KD, Pilgram T, Hsu CY. Temporal relationship between apparent diffusion coefficient and absolute measurements of cerebral blood flow in acute stroke patients. Stroke 2003; 34(1): 64-70.
18. Kane I, Hand PJ, Rivers C, Armitage P, Bastin ME, Lindley R, Dennis M, Wardlaw JM. A practical assessment of magnetic resonance diffusion-perfusion mismatch in acute stroke: observer variation and outcome. J Neurol 2009.
19. Ostergaard L, Jonsdottir KY, Mouridsen K. Predicting tissue outcome in stroke: new approaches. Curr Opin Neurol 2009; 22(1): 54-59.
20. Knutsson L, Borjesson S, Larsson EM, Risberg J, Gustafson L, Passant U, Stahlberg F, Wirestam R. Absolute quantification of cerebral blood flow in normal volunteers: correlation between Xe-133 SPECT and dynamic susceptibility contrast MRI. J Magn Reson Imaging 2007; 26(4): 913-920.
21. Mukherjee P, Kang HC, Videen TO, McKinstry RC, Powers WJ, Derdeyn CP. Measurement of cerebral blood flow in chronic carotid occlusive disease: comparison of dynamic susceptibility contrast perfusion MR imaging with positron emission tomography. AJNR Am J Neuroradiol 2003; 24(5): 862-871.
22. Shin W, Horowitz S, Ragin A, Chen Y, Walker M, Carroll TJ. Quantitative cerebral perfusion using dynamic susceptibility contrast MRI: evaluation of reproducibility and age- and gender-dependence with fully automatic image postprocessing algorithm. Magn Reson Med 2007; 58(6): 1232-1241.
23. Shin W, Cashen TA, Horowitz SW, Sawlani R, Carroll TJ. Quantitative CBV measurement from static T1 changes in tissue and correction for intravascular water exchange. Magn Reson Med 2006; 56(1): 138-145.
24. Lu H, Law M, Johnson G, Ge Y, van Zijl PC, Helpern JA. Novel approach to the measurement of absolute cerebral blood volume using vascular-space-occupancy magnetic resonance imaging. Magn Reson Med 2005; 54(6): 1403-1411.
25. Meier P,Zierler KL. On the theory of the indicator-dilution method for measurement of blood flow and volume. J Appl Physiol 1954; 6(12): 731-744.
26. Weisskoff RM, Chesler D, Boxerman JL, Rosen BR. Pitfalls in MR measurement of tissue blood flow with intravascular tracers: which mean transit time? Magn Reson Med 1993; 29(4): 553-558.
27. Fisel CR, Ackerman JL, Buxton RB, Garrido L, Belliveau JW, Rosen BR, Brady TJ. MR contrast due to microscopically heterogeneous magnetic susceptibility: numerical simulations and applications to cerebral physiology. Magn Reson Med 1991; 17(2): 336-347.
28. Guckel F, Brix G, Rempp K, Deimling M, Rother J, Georgi M. Assessment of cerebral blood volume with dynamic susceptibility contrast enhanced gradient-echo imaging. J Comput Assist Tomogr 1994; 18(3): 344-351.

29. Wirestam R, Andersson L, Ostergaard L, Bolling M, Aunola JP, Lindgren A, Geijer B, Holtas S, Stahlberg F. Assessment of regional cerebral blood flow by dynamic susceptibility contrast MRI using different deconvolution techniques. Magn Reson Med 2000; 43(5): 691-700.
30. Zierler KL. Theoretical Basis of Indicator-Dilution Methods for Measuring Flow and Volume. Circ. Res 1962; 10: 393-407.
31. Chen JJ, Smith MR, Frayne R. The impact of partial-volume effects in dynamic susceptibility contrast magnetic resonance perfusion imaging. J Magn Reson Imaging 2005; 22(3): 390-399.
32. Thijs VN, Somford DM, Bammer R, Robberecht W, Moseley ME, Albers GW. Influence of arterial input function on hypoperfusion volumes measured with perfusion-weighted imaging. Stroke 2004; 35(1): 94-98.
33. Kiselev VG. On the theoretical basis of perfusion measurements by dynamic susceptibility contrast MRI. Magn Reson Med 2001; 46(6): 1113-1122.
34. Kjolby BF, Mikkelsen IK, Pedersen M, Ostergaard L, Kiselev VG. Analysis of partial volume effects on arterial input functions using gradient echo: a simulation study. Magn Reson Med 2009; 61(6): 1300-1309.
35. Rausch M, Scheffler K, Rudin M, Radu EW. Analysis of input functions from different arterial branches with gamma variate functions and cluster analysis for quantitative blood volume measurements. Magn Reson Imaging 2000; 18(10): 1235-1243.
36. Ellinger R, Kremser C, Schocke MF, Kolbitsch C, Griebel J, Felber SR, Aichner FT. The impact of peak saturation of the arterial input function on quantitative evaluation of dynamic susceptibility contrast-enhanced MR studies. J Comput Assist Tomogr 2000; 24(6): 942-948.
37. Buxton RB, Frank LR, Wong EC, Siewert B, Warach S, Edelman RR. A general kinetic model for quantitative perfusion imaging with arterial spin labeling. Magn Reson Med 1998; 40(3): 383-396.
38. Petersen ET, Lim T, Golay X. Model-free arterial spin labeling quantification approach for perfusion MRI. Magn Reson Med 2006; 55(2): 219-232.
39. Herscovitch P RM. What is the correct value for the brain-blood partition coefficient for water? J Cereb Blood Flow Metab 1985; 5: 65-69.
40. Warntjes JB, Dahlqvist O, Lundberg P. Novel method for rapid, simultaneous T1, T*2, and proton density quantification. Magn Reson Med 2007; 57(3): 528-537.
41. Wu O, Ostergaard L, Weisskoff RM, Benner T, Rosen BR, Sorensen AG. Tracer arrival timing-insensitive technique for estimating flow in MR perfusion-weighted imaging using singular value decomposition with a block-circulant deconvolution matrix. Magn Reson Med 2003; 50(1): 164-174.
42. Thilmann O. LUPE: an extensible modular framework for evaluation of DSC-acquired perfusion images. Magn Reson Mater Phy 2004; 16: 537.
43. Lu H, Law M, Ge Y, Hesseltine SM, Rapalino O, Jensen JH, Helpern JA. Quantitative measurement of spinal cord blood volume in humans using vascular-space-occupancy MRI. NMR Biomed 2008; 21(3): 226-232.
44. van Gelderen P, de Zwart JA, Duyn JH. Pittfalls of MRI measurement of white matter perfusion based on arterial spin labeling. Magn Reson Med 2008; 59(4): 788-795.
45. Ito H, Kanno I, Kato C, Sasaki T, Ishii K, Ouchi Y, Iida A, Okazawa H, Hayashida K, Tsuyuguchi N, Kuwabara Y, Senda M. Database of normal human cerebral blood flow, cerebral blood volume, cerebral oxygen extraction fraction and cerebral metabolic rate of oxygen measured by positron emission tomography with 15O-

labelled carbon dioxide or water, carbon monoxide and oxygen: a multicentre study in Japan. Eur J Nucl Med Mol Imaging 2004; 31(5): 635-643.
46. Rostrup E, Law I, Pott F, Ide K, Knudsen GM. Cerebral hemodynamics measured with simultaneous PET and near-infrared spectroscopy in humans. Brain Res 2002; 954(2): 183-193.
47. von Oettingen G, Bergholt B, Ostergaard L, Jensen LC, Gyldensted C, Astrup J. Xenon CT cerebral blood flow in patients with head injury: influence of pulmonary trauma on the input function. Neuroradiology 2000; 42(3): 168-173.
48. Uh J, Lewis-Amezcua K, Varghese R, Lu H. On the measurement of absolute cerebral blood volume (CBV) using vascular-space-occupancy (VASO) MRI. Magn Reson Med 2009; 61(3): 659-667.
49. Petersen ET, Mouridsen K, Golay X. The QUASAR reproducibility study, Part II: Results from a multi center Arterial Spin Labeling test-retest Study. Neuroimage 2009.
50. H. Kamano TY, A. Hiwatashi, K. Yamashita, E. Nagao, Y. Takayama, T. Noguchi, K. Abe, K. Kaneko, I. Zimine, T. Okuaki, and H. Honda. Cerebral Blood Flow and Transit Time Measured by Quantitative Arterial Spin Labeling: Comparison with 15O-PET. In Book of abstracts Proc 17th Intl Soc Magn Reson Med p.34

51. Y. Uchihashi KH, I. Zimine, A. Fujita, S. Inoue, H. Aihara, H. Kawamitsu, N. Aoyama, H. Aoki, M. Fujii, and E. Kohmura. Comparison of CBF measurement by ASL and SPECT in Patients with Internal Carotid Artery Stenosis. In Book of abstracts Proc 17th Intl Soc Magn Reson Med p.3643

Appendix

Table A 1. CBVss values and calibration factors from Bookend measurements. Subject number 2 was excluded due to technical problems.

Subject	CBVss WM (Bookend) [ml/100g]	Bookend CF based on WM	CBVss GM (Bookend) [ml/100 g]	Bookend CF based on GM
1	0.8	0.06	2.8	0.15
2	NA	NA	NA	NA
3	1.2	0.11	3.2	0.15
4	0.2	0.01	1.0	0.04
5	1.2	0.09	2.3	0.11
6	1.6	0.05	3.0	0.08
7	1.1	0.09	0.6	0.03
8	1.1	0.10	2.6	0.12
9	1.9	0.12	2.8	0.12
10	1.3	0.09	1.2	0.06
11	1.9	0.18	3.5	0.15
12	1.4	0.08	2.8	0.10
13	1.1	0.06	2.8	0.11
14	2.2	0.14	3.0	0.13
Mean value	1.3	0.09	2.4	0.10
Standard deviation	0.5	0.04	0.9	0.04

NA – not available

Table A 2. CBVss values and calibration factors from VASO measurements.

Subject	CBVss WM (VASO) [ml/100g]	VASO CF based on WM	CBVss GM (VASO) [ml/100 g]	VASO CF based on GM
1	1.3	0.16	1.9	0.15
2	1.9	0.16	3.0	0.15
3	1.6	0.15	3.0	0.16
4	1.2	0.08	2.4	0.13
5	1.2	0.10	2.5	0.13
6	1.6	0.10	2.9	0.10
7	1.3	0.08	2.2	0.13
8	1.8	0.13	2.1	0.15
9	0.9	0.08	2.2	0.16
10	2.0	0.20	3.1	0.23
11	1.7	0.18	2.6	0.13
12	1.3	0.10	2.6	0.09
13	1.1	0.09	2.7	0.14
14	1.6	0.12	2.0	0.12
Mean value	1.5	0.12	2.5	0.14
Standard deviation	0.3	0.04	0.4	0.03

Table A 3. CBV values in white matter after application of calibration factors from Bookend and VASO

Subject	WM CBV [ml/100 g] Bookend CF from WM	WM CBV [ml/100 g] Bookend CF from GM	WM CBV [ml/100 g] VASO CF from WM	WM CBV [ml/100 g] VASO CF from GM
1	0.4	0.9	0.9	0.8
2	NA	NA	1.1	1.0
3	1.2	1.6	1.7	1.7
4	0.1	0.3	0.5	0.9
5	1.2	1.6	1.5	1.8
6	1.2	1.8	2.3	2.2
7	1.1	0.4	1.0	1.6
8	0.7	0.9	1.0	1.1
9	1.1	1.1	0.7	1.5
10	0.7	0.5	1.5	1.7
11	1.5	1.3	1.6	1.1
12	0.6	0.9	0.8	0.8
13	0.6	1.1	0.8	1.3
14	1.4	1.4	1.2	1.2
Mean value	0.9	1.0	1.2	1.3
Standard deviation	0.4	0.5	0.5	0.4

Table A 4. CBV values in grey matter after application of calibration factors from Bookend and VASO

Subject	GM CBV [ml/100 g] Booken CF from WM	GM CBV [ml/100 g] Bookend CF from GM	GM CBV [ml/100 g] VASO CF from WM	GM CBV [ml/100 g] VASO CF from GM
1	1.1	2.6	2.9	2.6
2	NA	NA	3.6	3.3
3	2.1	2.8	2.9	3.0
4	0.3	1.0	1.9	3.3
5	1.6	2.1	2.0	2.4
6	2.2	3.3	4.2	4.2
7	1.5	0.5	1.4	2.1
8	1.4	1.7	1.9	2.1
9	2.2	2.2	1.4	3.0
10	1.2	0.7	2.5	2.8
11	2.4	1.9	2.4	1.7
12	1.7	2.3	2.2	2.0
13	1.1	2.1	1.6	2.5
14	4.2	4.0	3.6	3.6
Mean value	1.8	2.1	2.5	2.8
Standard deviation	0.9	1.0	0.9	0.7

Table A 5. CBF values in white matter after application of calibration factors from Bookend and VASO

Subject	WM CBF [ml/(min· 100 g)] Bookend CF from WM	WM CBF [ml/(min· 100 g)] Bookend CF from GM	WM CBF [ml/(min· 100 g)] VASO CF from WM	WM CBF [ml/(min· 100 g)] VASO CF from GM
1	3.4	8.0	8.7	8.0
2	NA	NA	11	10
3	10	13	14	14
4	0.6	1.7	3.4	5.8
5	11	14	13	16
6	17	26	33	32
7	6.5	2.3	6.1	9.3
8	7.6	9.4	10	11
9	10	10	6.3	13
10	7.8	5.0	17	19
11	12	10	12	9.1
12	10	13	13	11
13	5.4	10	7.5	12
14	12	11	10	10
Mean value	8.7	10	12	13
Standard deviation	4.2	6.0	7.1	6.5

Table A 6. CBF values in grey matter after application of calibration factors from Bookend and VASO

Subject	GM CBF [ml/(min· 100 g)] Bookend CF from WM	GM CBF [ml/(min· 100 g)] Bookend CF from GM	GM CBF [ml/(min· 100 g)] VASO CF from WM	GM CBF [ml/(min· 100 g)] VASO CF from GM
1	13	30	33	30
2	NA	NA	33	31
3	30	39	41	42
4	3.1	8.5	17	29
5	20	26	24	30
6	31	48	62	60
7	16	5.7	15	24
8	20	24	27	29
9	33	32	21	45
10	16	10	34	39
11	35	29	35	26
12	21	29	28	25
13	15	27	21	33
14	43	40	36	37
Mean value	23	27	31	34
Standard deviation	11	13	12	10

Table A 7. MTT in white and grey matter obtained from non-calibrated DSC-MRI measurements

Subject	MTT [s] WM	MTT [s] GM
1	6.3	4.9
2	5.8	5.7
3	7.1	4.0
4	8.5	6.1
5	6.5	4.4
6	5.1	3.9
7	9.8	4.8
8	5.7	3.7
9	6.5	3.5
10	5.4	3.9
11	6.9	3.5
12	3.5	3.7
13	7.1	4.0
14	6.9	5.5
Mean value	6.5	4.4
Standard deviation	1.5	0.9

Table A 8. CBF values in cortical grey matter obtained by ASL and DSC-MRI. DSC-MRI values are extracted from non-calibrated images as well as from images calibrated using grey- and white-matter based calibration factors from Bookend and VASO

Subject	ASL CBF [ml/(min· 100 g)] from ASL	Non-calibrated DSC-MRI CBF [ml/(min· 100 g)]	Bookend CF from WM CBF [ml/(min· 100 g)]	Bookend CF from GM CBF [ml/(min· 100 g)]	VASO CF from WM CBF [ml/(min· 100 g)]	VASO CF from GM CBF [ml/(min· 100 g)]
1	44	231	14	34	37	34
2	37	281	NA	NA	44	41
3	43	259	29	38	40	41
4	41	241	3.4	9.5	19	32
5	26	300	26	34	31	39
6	50	537	29	43	56	55
7	28	250	22	7.8	21	32
8	34	214	21	26	29	31
9	61	322	38	37	25	51
10	45	279	26	17	55	63
11	60	361	64	53	65	48
12	52	447	34	47	45	41
13	49	360	22	41	31	49
14	44	306	42	39	35	36
Mean value	44	313	29	33	38	42
Standard deviation	10	89	15	14	14	10

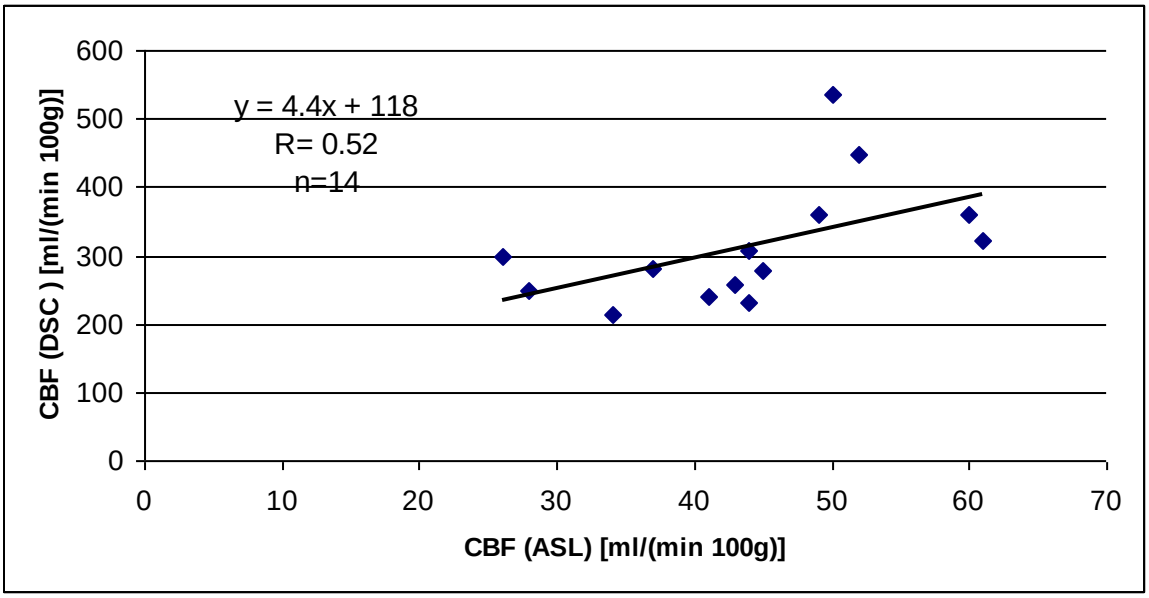

Figure A 1. Relationship between CBF estimates in cortical grey matter obtained by ASL and non-calibrated DSC-MRI.

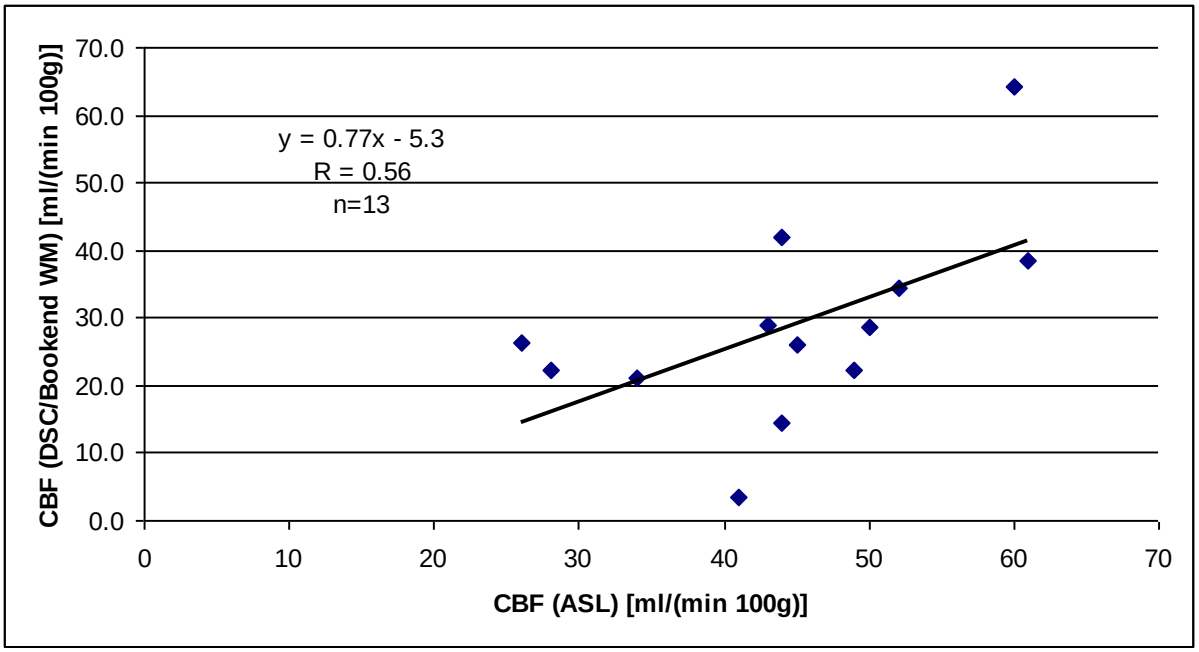

Figure A 2. Relationship between CBF estimates in cortical grey matter, obtained by ASL and DSC-MRI with a Bookend calibration factor from white matter.

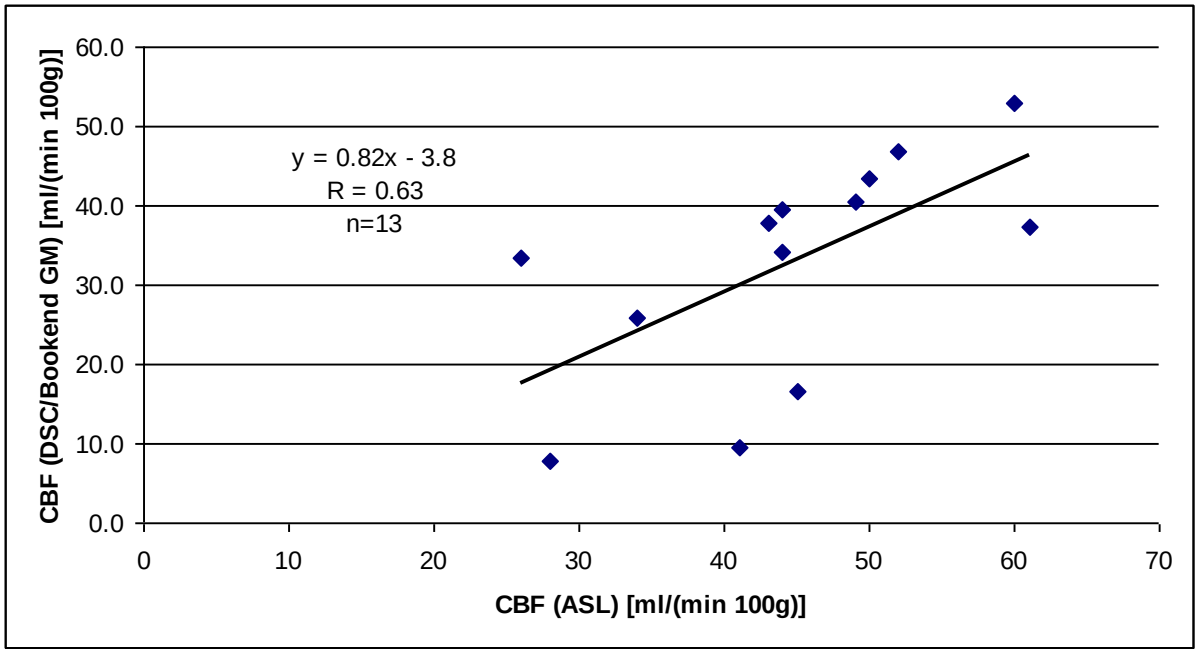

Figure A 3. Relationship between CBF estimates in cortical grey matter, obtained by ASL and DSC-MRI with a Bookend calibration factor from grey matter.

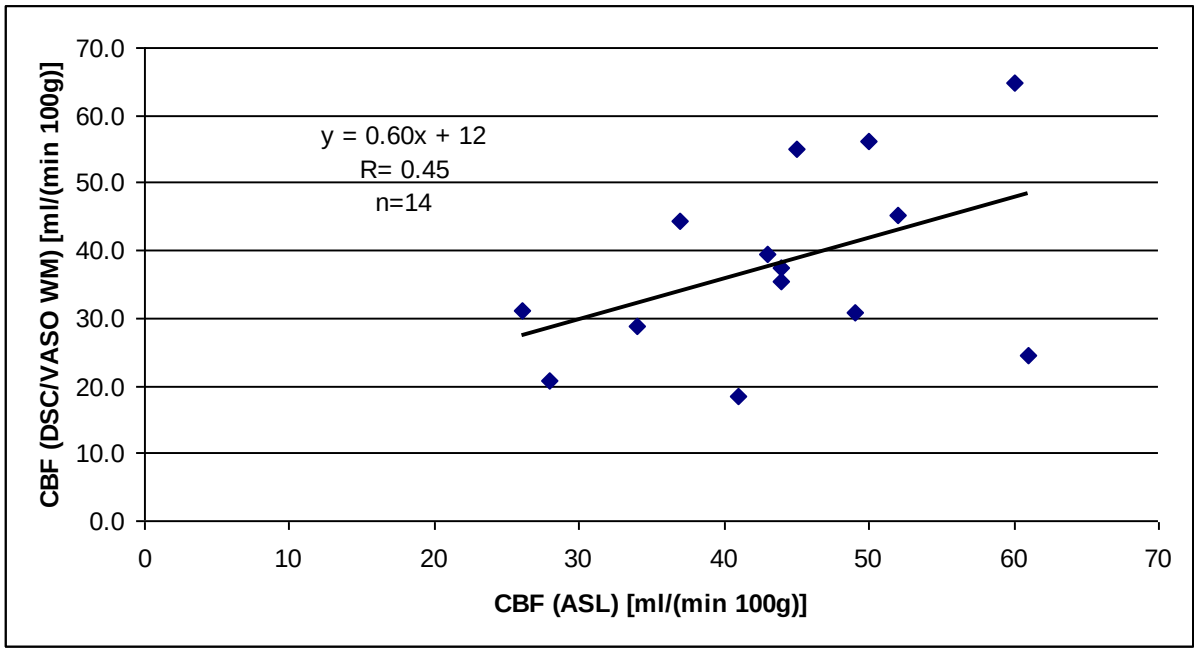

Figure A 4. Relationship between CBF estimates in cortical grey matter, obtained by ASL and DSC-MRI with a VASO calibration factor from white matter.

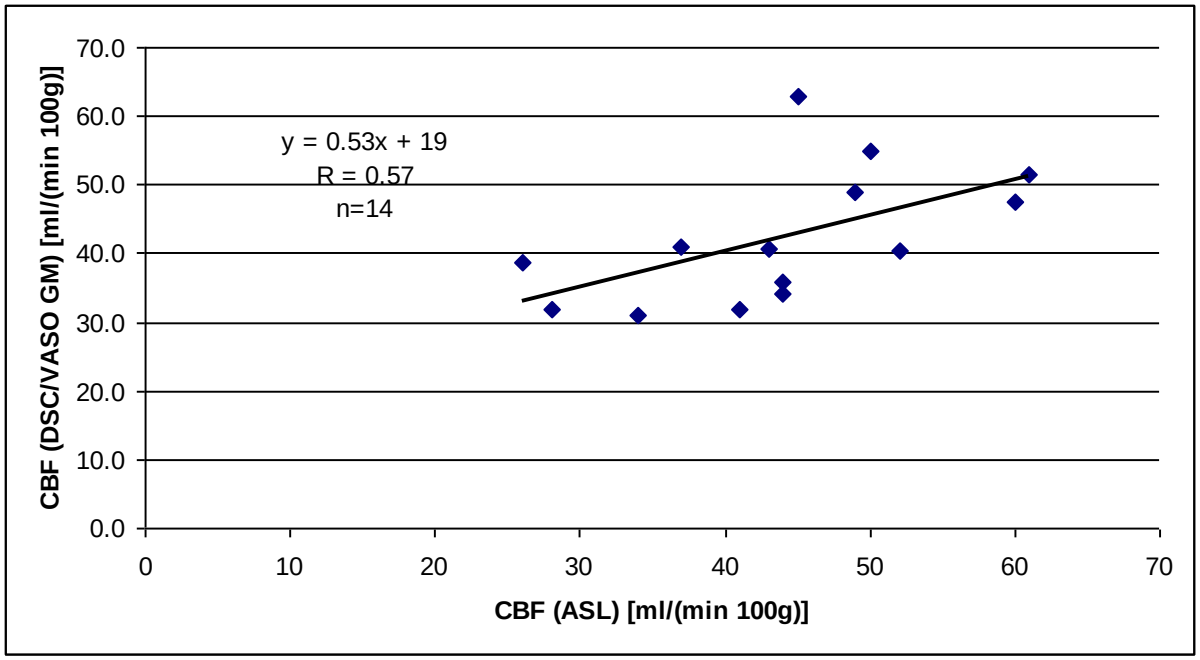

Figure A 5. Relationship between CBF estimates in cortical grey matter, obtained by ASL and DSC-MRI with a VASO calibration factor from grey matter.

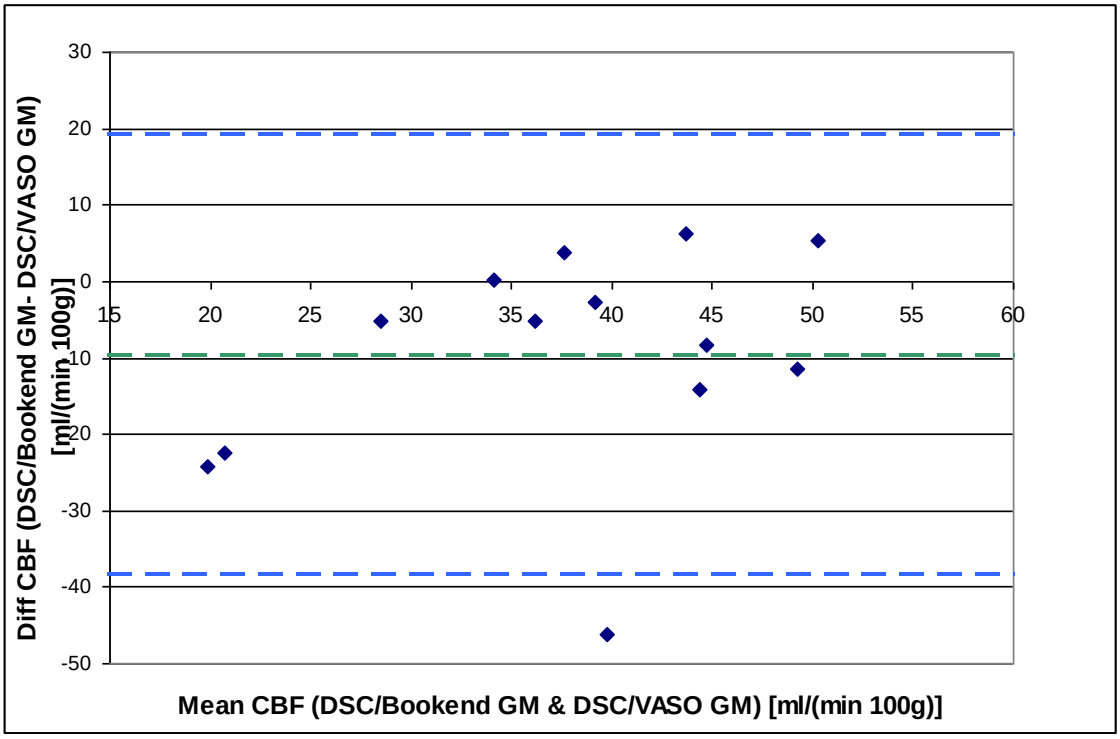

Figure A 6. Bland-Altman analysis of GM CBF estimates obtained using the Bookend and the VASO calibration methods. Calibration factors are based on GM regions. The dashed green line is the mean difference between the two populations and the dashed blue lines are mean±1.96·SD.

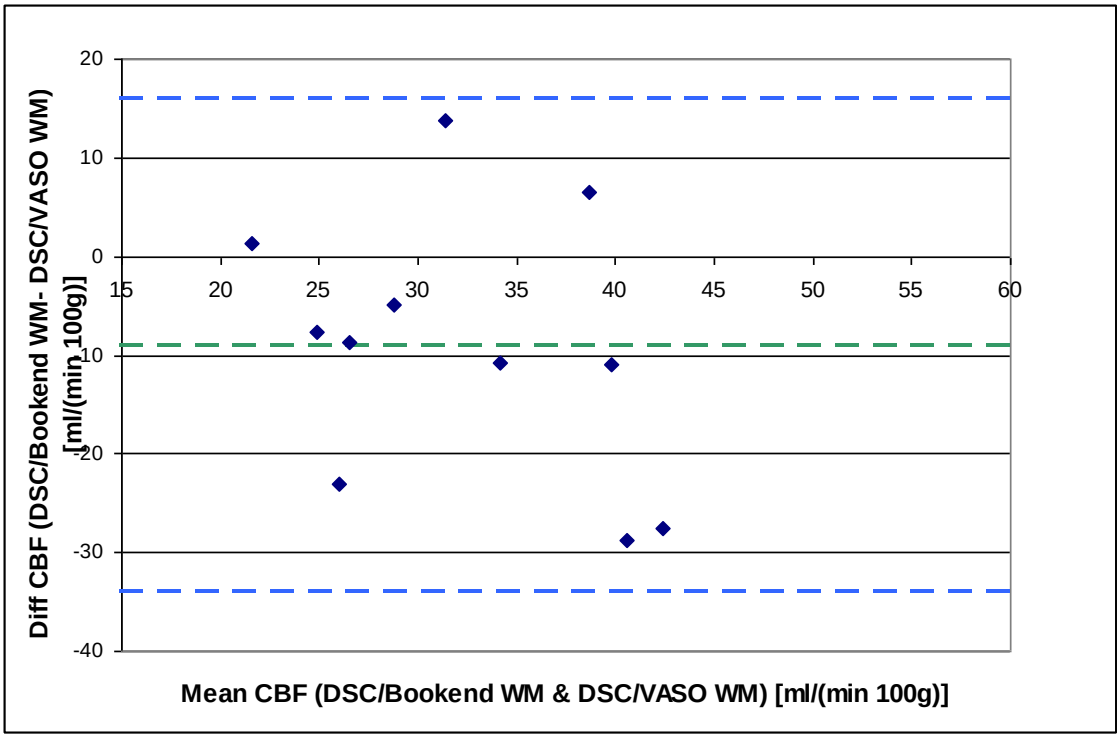

Figure A 7. Bland-Altman analysis of GM CBF estimates obtained using the Bookend and the VASO calibration methods. Calibration factors are based on WM regions. The dashed green line is the mean difference between the two populations and the dashed blue lines are mean±1.96·SD.

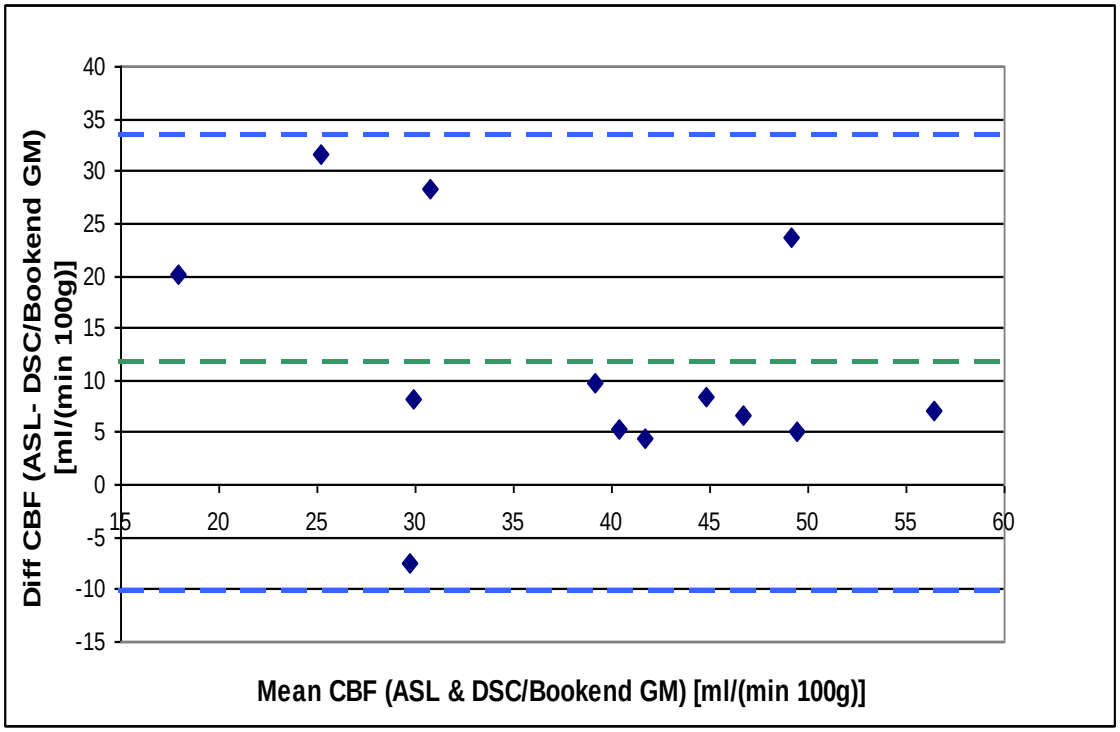

Figure A 8. Bland-Altman analysis of GM CBF estimates obtained using the ASL and the Bookend calibration methods. Calibration factors are based on GM regions. The dashed green line is the mean difference between the two populations and the dashed blue lines are mean±1.96·SD.

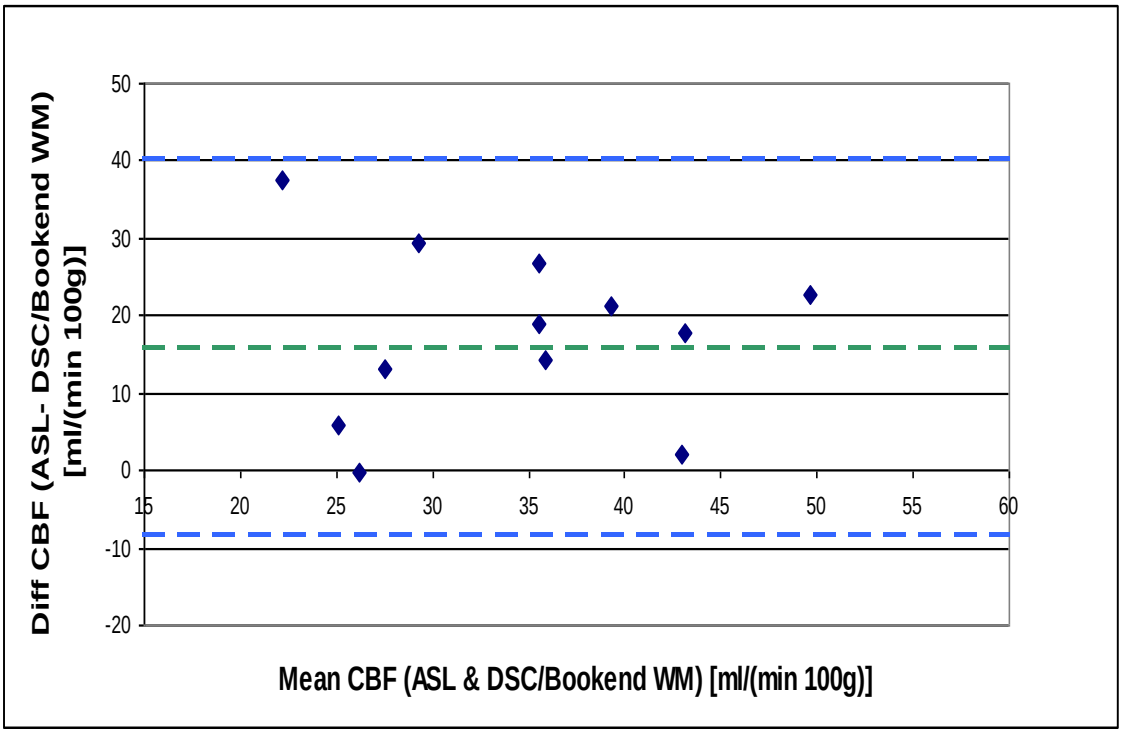

Figure A 9. Bland-Altman analysis of GM CBF estimates obtained using ASL and the Bookend calibration methods. Calibration factors are based on WM regions. The dashed green line is the mean difference between the two populations and the dashed blue lines are mean±1.96·SD.

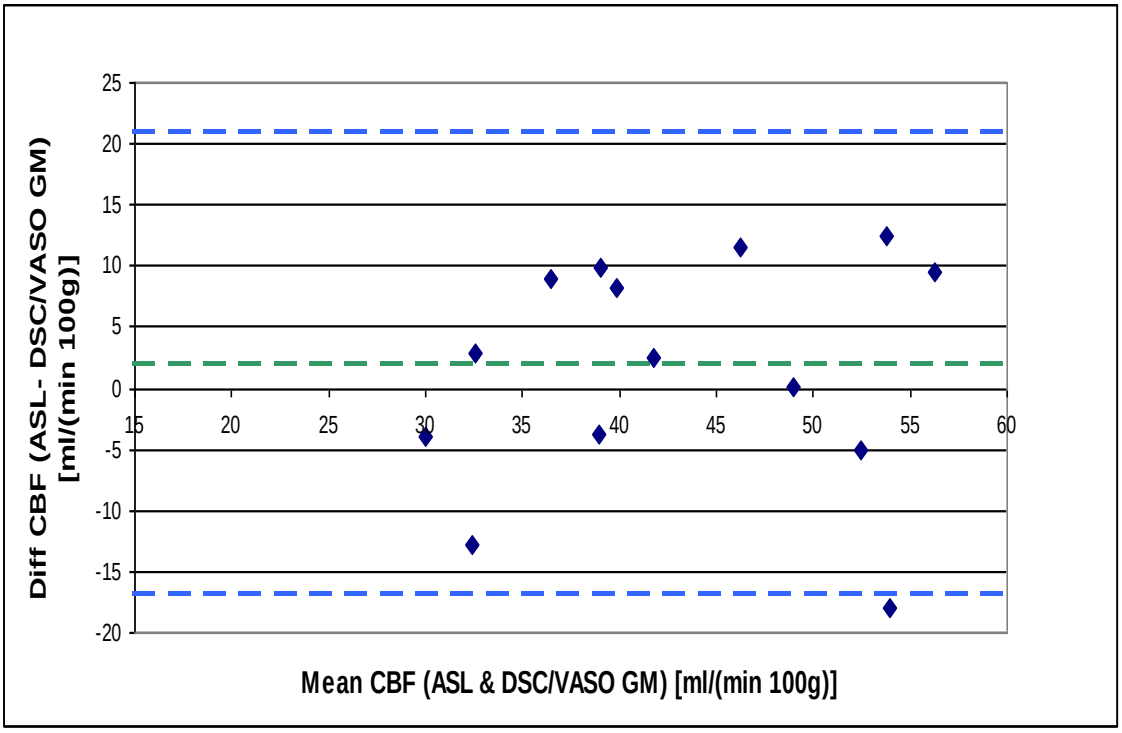

Figure A 10. Bland-Altman analysis of GM CBF estimates obtained using ASL and the VASO calibration methods. Calibration factors are based on GM regions. The dashed green line is the mean difference between the two populations and the dashed blue lines are mean±1.96·SD.

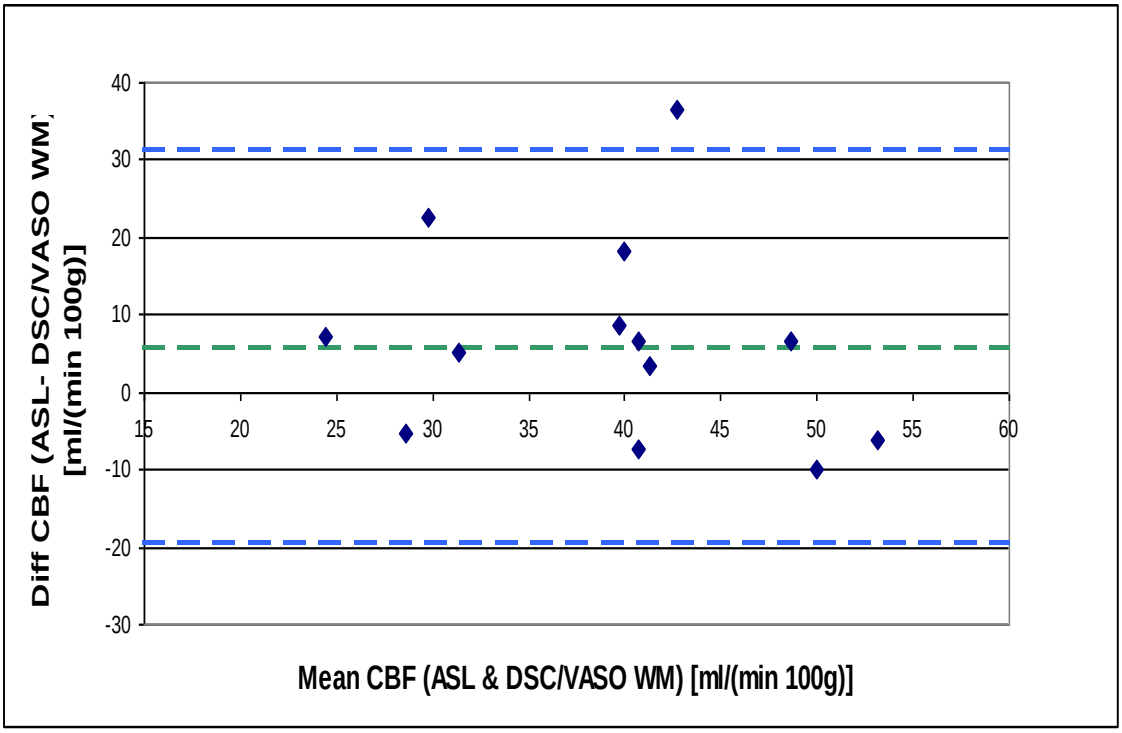

Figure A 11. Bland-Altman analysis of GM CBF estimates obtained using ASL and the VASO calibration methods. Calibration factors are based on WM regions. The dashed green line is the mean difference between the two populations and the dashed blue lines are mean±1.96·SD.